Prediction of physical fields under linear equality constraints

Enbis-26 conference, September the 8th , 2026

NASSOURADINE MAHAMAT HAMDAN[1,2]

Supervisors : **Clément Gauchy**[1]**, Pierre-Emmanuel Angeli**[1]
PhD Director : **Sébastien Da Veiga**[2]

mahamat-hamdan.nassouradine@cea.fr
CEA Saclay[1] ENSAI CREST[2]

Motivation

- **Verification & Validation of CFD simulators (VVUQ)**

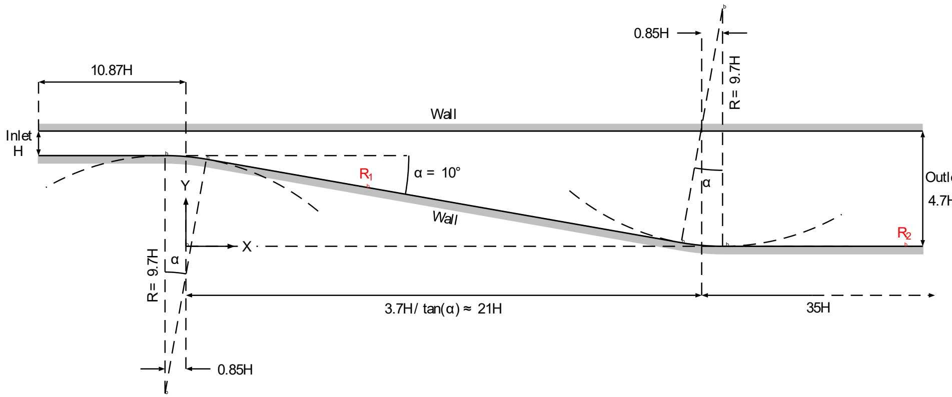

Figure: Scheme of the experiment carried out in Buice and Eaton, 2000.

Motivation

- **Verification & Validation of CFD simulators (VVUQ)**

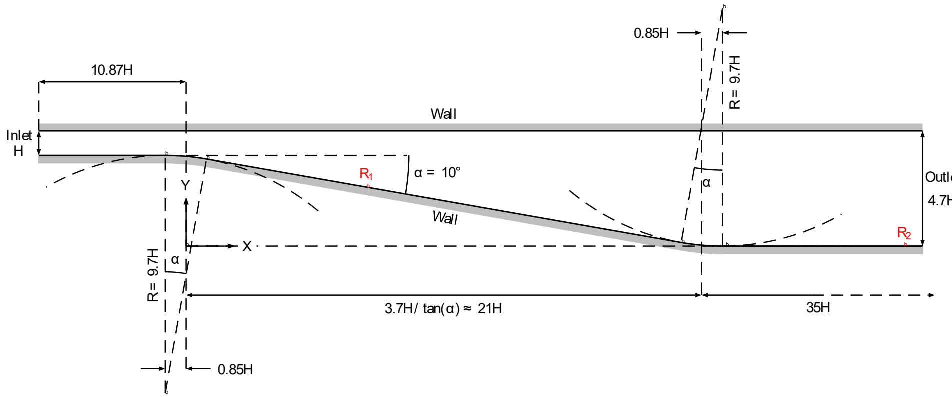

Figure: Scheme of the experiment carried out in Buice and Eaton, 2000.

↓

Computer code

$$\mathcal{M} : \mathcal{X} \to \mathbb{R}^P$$

(RANS solver with **Trio-CFD**)

Motivation

- **Verification & Validation of CFD simulators (VVUQ)**

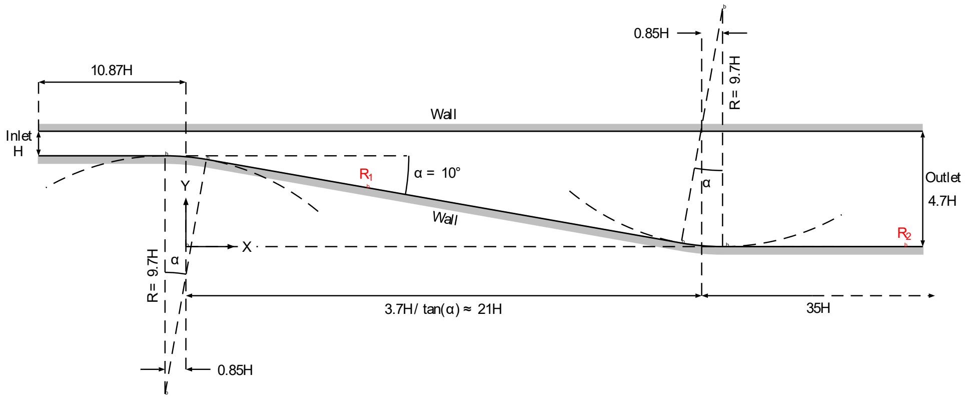

Figure: Scheme of the experiment carried out in Buice and Eaton, 2000.

Computer code

$$\mathcal{M} : \mathcal{X} \to \mathbb{R}^P$$

(RANS solver with **Trio-CFD**)

Outputs $\in \mathbb{R}^S$

$S \approx 140\ 000$: **mesh size**

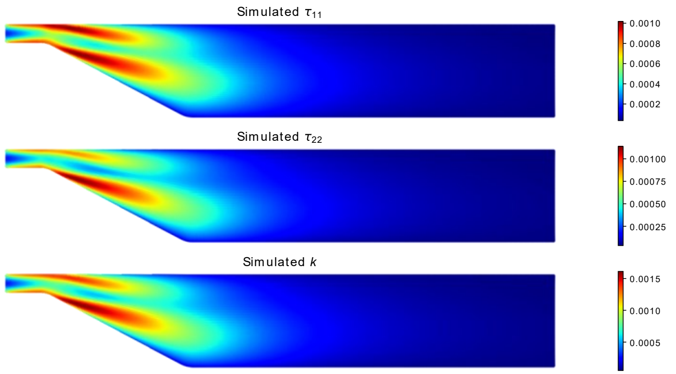

Motivation

- **Verification & Validation of CFD simulators (VVUQ)**

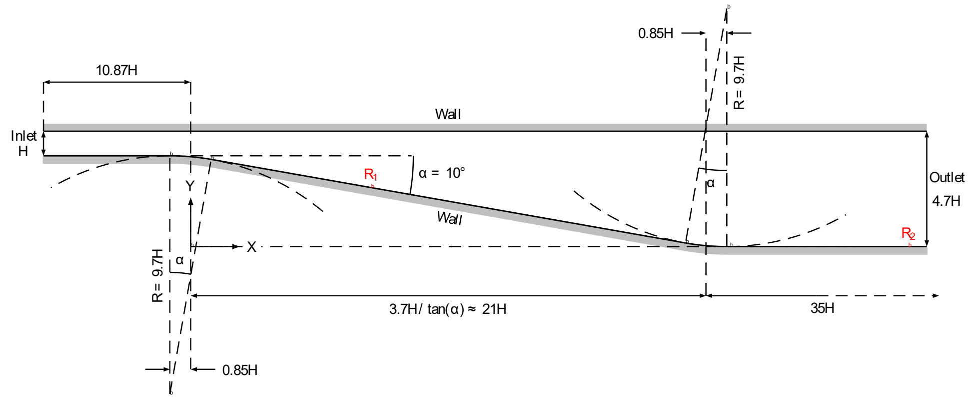

Figure: Scheme of the experiment carried out in Buice and Eaton, 2000.

Input

Closure coefficients of the RANS model:
$\boldsymbol{x} = (C_\mu, \sigma_k, \sigma_\varepsilon, C_{\varepsilon_1}, C_{\varepsilon_2})$

Computer code

$\mathcal{M} : \mathcal{X} \to \mathbb{R}^P$

(RANS solver with **Trio-CFD**)

Outputs $\in \mathbb{R}^S$
$S \approx 140\ 000$: mesh size

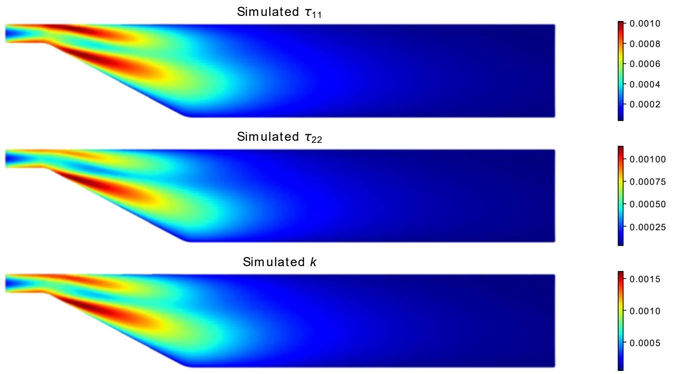

Motivation

- **Verification & Validation of CFD simulators (VVUQ)**

☛ **Goal: Validation of $\mathcal{M}$**

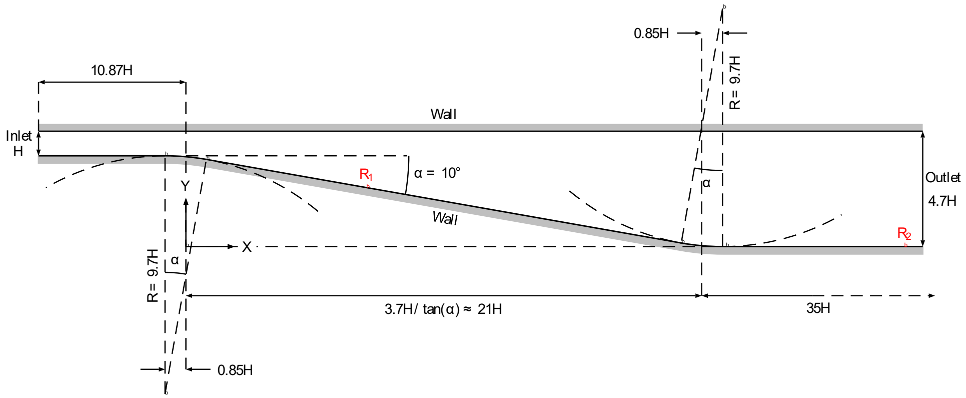

Figure: Scheme of the experiment carried out in Buice and Eaton, 2000.

Input

Closure coefficients of the RANS model:
$\boldsymbol{x} = (C_\mu, \sigma_k, \sigma_\varepsilon, C_{\varepsilon_1}, C_{\varepsilon_2})$

Computer code

$\mathcal{M} : \mathcal{X} \to \mathbb{R}^P$

(RANS solver with **Trio-CFD**)

Outputs $\in \mathbb{R}^S$
$S \approx 140\ 000$: mesh size

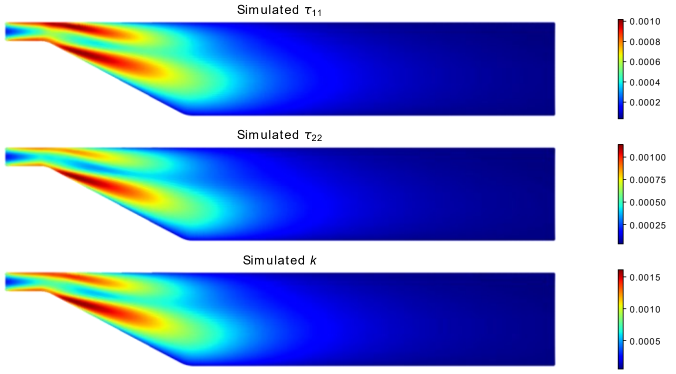

Motivation

- **Verification & Validation of CFD simulators (VVUQ)**

Goal: Validation of $\mathcal{M}$

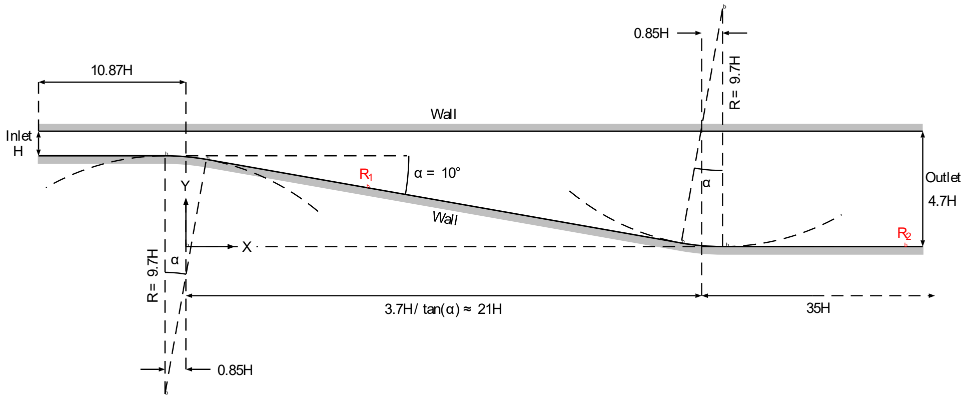

Figure: Scheme of the experiment carried out in Buice and Eaton, 2000.

Input

Closure coefficients
of the RANS model:
$\boldsymbol{x} = (C_\mu, \sigma_k, \sigma_\varepsilon, C_{\varepsilon_1}, C_{\varepsilon_2})$

Computer code

$\mathcal{M} : \mathcal{X} \to \mathbb{R}^P$

(RANS solver with **Trio-CFD**)

× **Computationally expensive !**

Outputs $\in \mathbb{R}^S$
$S \approx 140\ 000$: mesh size

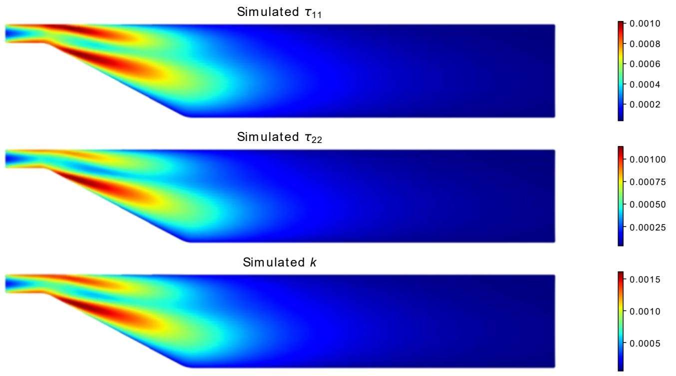

Motivation

- **Verification & Validation of CFD simulators (VVUQ)**

Goal: Validation of $\mathcal{M}$

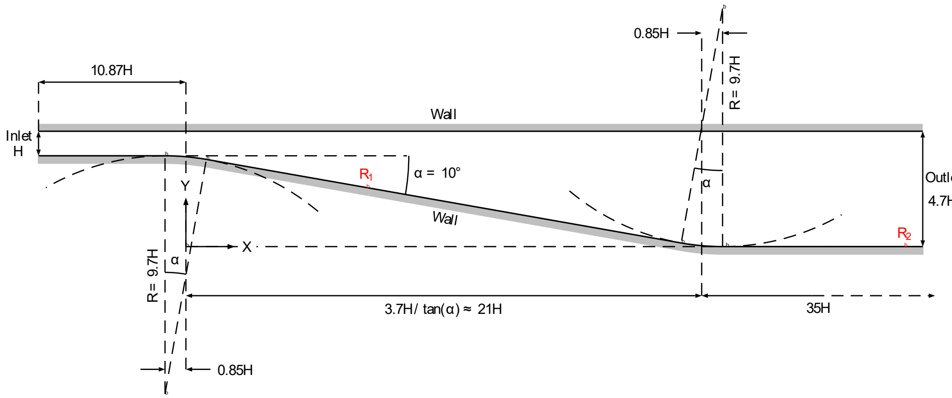

Figure: Scheme of the experiment carried out in Buice and Eaton, 2000.

Input

Closure coefficients of the RANS model: $\boldsymbol{x} = (C_\mu, \sigma_k, \sigma_\varepsilon, C_{\varepsilon_1}, C_{\varepsilon_2})$

Computer code

$\mathcal{M} : \mathcal{X} \to \mathbb{R}^P$

(RANS solver with **Trio-CFD**)

× **Computationally expensive !**

Outputs $\in \mathbb{R}^S$

$S \approx 140\ 000$: mesh size

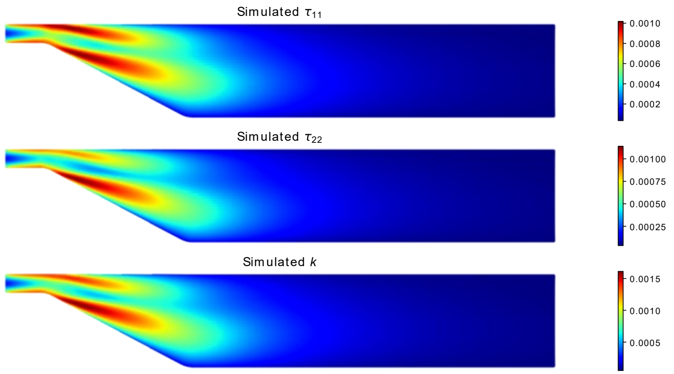

Solution: Build a metamodel $\widehat{\mathcal{M}}$

Motivation

- **Verification & Validation of CFD simulators (VVUQ)**

Goal: Validation of $\mathcal{M}$

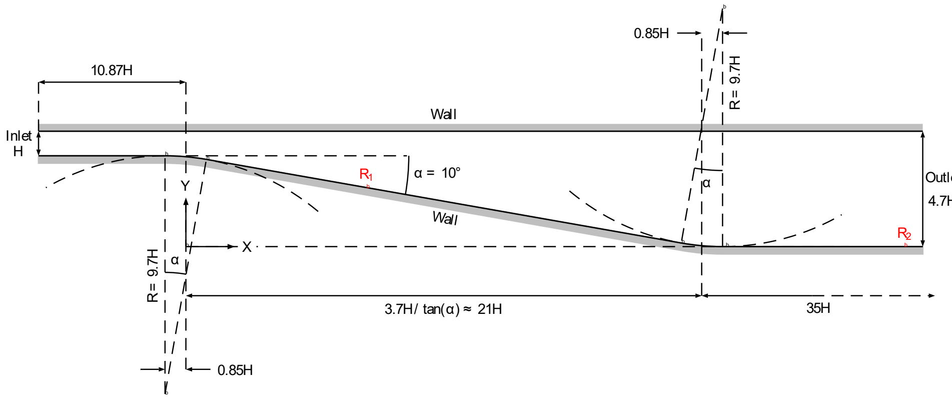

Figure: Scheme of the experiment carried out in Buice and Eaton, 2000.

Input

Closure coefficients of the RANS model: $\boldsymbol{x} = (C_\mu, \sigma_k, \sigma_\varepsilon, C_{\varepsilon_1}, C_{\varepsilon_2})$

Computer code

$$\mathcal{M} : \mathcal{X} \to \mathbb{R}^P$$

(RANS solver with **Trio-CFD**)

× **Computationally expensive !**

Solution: Build a metamodel $\widehat{\mathcal{M}}$

Outputs $\in \mathbb{R}^S$

$S \approx 140\ 000$: mesh size

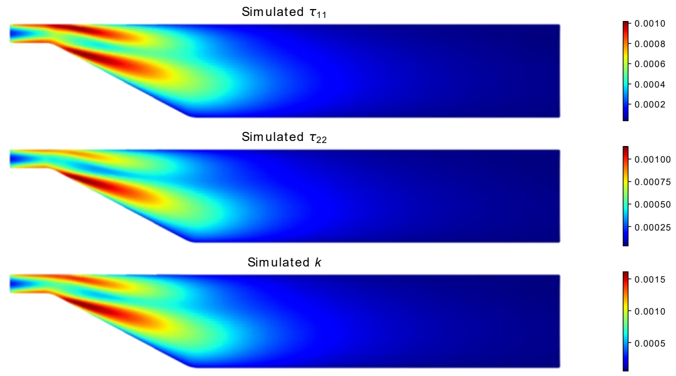

× **High dimensional multi-field outputs!**

× **Physical constraints !**

Physics constraints for incompressible flows

Many physics problems are governed by linear constraints, for example:

- The law of conservation of mass implies linear relationships between the concentrations or proportions of different chemical species in a given solution

Physics constraints for incompressible flows

Many physics problems are governed by linear constraints, for example:

- The law of conservation of mass implies linear relationships between the concentrations or proportions of different chemical species in a given solution
- The incompressibility condition in fluid dynamics leads to linear constraints on the velocity field or, equivalently, a zero-trace stress or strain tensor

$$\boldsymbol{y}(\boldsymbol{x}) = [\boldsymbol{\tau}_{11}(\boldsymbol{x}), \boldsymbol{\tau}_{22}(\boldsymbol{x}), \boldsymbol{k}(\boldsymbol{x})]$$

$$P = 3 \times S$$

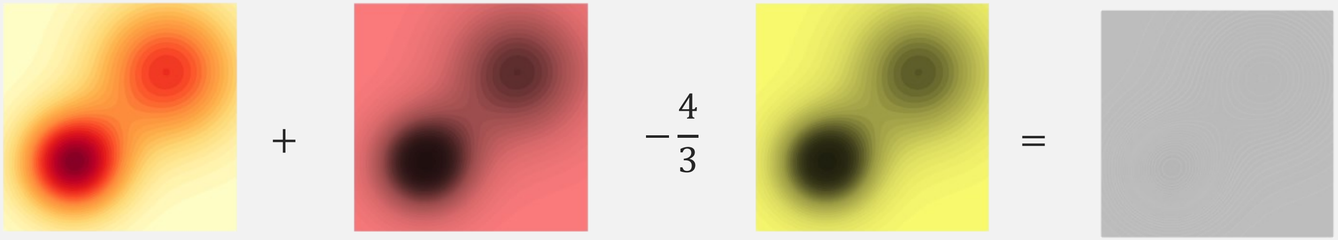

$$\boldsymbol{\tau}_{11}(\boldsymbol{x}) + \boldsymbol{\tau}_{22}(\boldsymbol{x}) - \frac{4}{3}\boldsymbol{k}(\boldsymbol{x}) = \boldsymbol{0}_S$$

$\boldsymbol{\tau}_{11}(\boldsymbol{x}) \in \mathbb{R}^S$ $\boldsymbol{\tau}_{22}(\boldsymbol{x}) \in \mathbb{R}^S$ $\boldsymbol{k}(\boldsymbol{x}) \in \mathbb{R}^S$ $\boldsymbol{0}_S \in \mathbb{R}^S$

Reynolds stress tensor $\tau_{ij} = \overline{u'_i u'_j}$ and the turbulent kinetic energy k

Linear constraints from physics

$$\boldsymbol{y}(\boldsymbol{x}) = [\boldsymbol{y}^{1}(\boldsymbol{x}), \dots, \boldsymbol{y}^{Q}(\boldsymbol{x})]$$
$$P = Q \times S$$

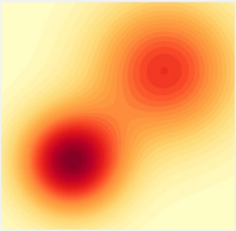

$\boldsymbol{y}^{1}(\boldsymbol{x}) \in \mathbb{R}^{S}$

…

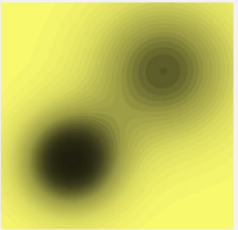

$\boldsymbol{y}^{Q}(\boldsymbol{x}) \in \mathbb{R}^{S}$

In this work, we are considering:

- An observed Q-dimensional vector field output on a fixed mesh of size S : $y_i = \left(y_i^1, \dots, y_i^Q\right) \in (\mathbb{R}^S)^Q$
- The vector output regression function to estimate: $f = (f^1, \dots, f^Q)\colon \mathcal{X} \longrightarrow (\mathbb{R}^S)^Q$

Linear constraints from physics

$$\boldsymbol{y}(\boldsymbol{x}) = [\boldsymbol{y}^1(\boldsymbol{x}), \dots, \boldsymbol{y}^Q(\boldsymbol{x})]$$
$$P = Q \times S$$

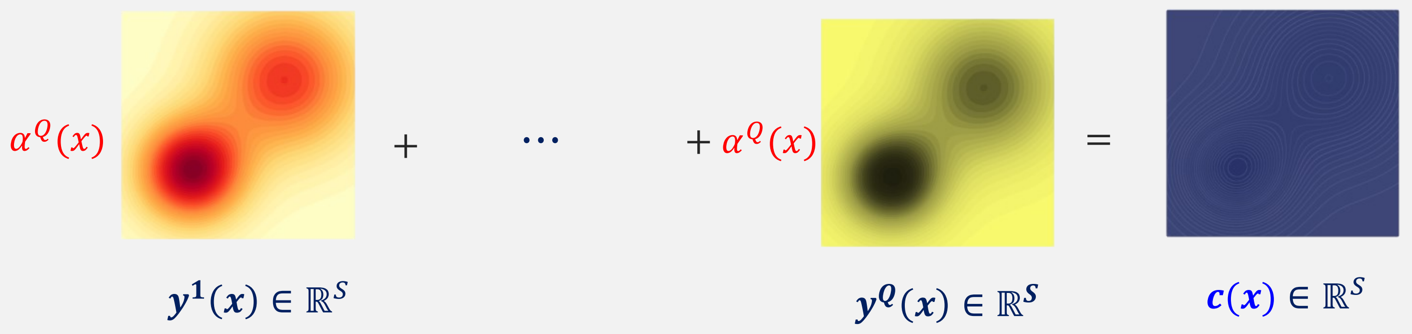

In this work, we are considering:

- An observed Q-dimensional vector field output on a fixed mesh of size S : $y_i = (y_i^1, \dots, y_i^Q) \in (\mathbb{R}^S)^Q$
- The vector output regression function to estimate: $f = (f^1, \dots, f^Q)$: $\mathcal{X} \longrightarrow (\mathbb{R}^S)^Q$
- The class of linear constraints defined through the sum of the Q scalar fields $f^j(.)$:

$$\mathcal{F}[f(x)] = \sum_{j=1}^{Q} \alpha^j(x) f^j(x) = c(x) \qquad (1)$$

where $\alpha^j(.)$ are input-dependent scalar weights, $f^j(.)$ and $c(.)$ are scalar fields. We assume α^j and c **are known**.

Problem statement

Simultaneous modeling of linearly constrained fields

We are considering the multi-output regression task of finding $f = (f_1, \dots, f_Q)$: $\mathcal{X} \longrightarrow \mathcal{Y}$, such that:

$$\begin{cases} y = f(x), \quad y \text{ is a high dimensional tensor, i.e. } P \approx 10^6 \\ \mathcal{F}[f(x)] = \sum_{j=1}^{Q} \alpha^j(x) f^j(x) = c(x) \end{cases}$$

Problem statement

Simultaneous modeling of linearly constrained fields

We are considering the multi-output regression task of finding $f = (f_1, \dots, f_Q)\colon \mathcal{X} \longrightarrow \mathcal{Y}$, such that:

$$\begin{cases} y = f(x), \qquad y \text{ is a high dimensional tensor, i.e. } P \approx 10^6 \\ \mathcal{F}[f(x)] = \sum_{j=1}^{Q} \alpha^j(x) f^j(x) = c(x) \end{cases}$$

Main mathematical tools:

- **Multi-output Gaussian process regression[1]**
  - ⟹ Suited for small data context
  - ⟹ Provides naturally uncertainty quantification with the prediction
  - ⟹ Can deal with constrained problems
  - × Not suited for high dimensional output
- **Principal component analysis**
  - ⟹ Linear and explicit reconstruction error

[1] Alvarez , M. A., Rosasco, L., & Lawrence, N. D. (2012)

Handling linear equality constraints

$$\sum_{j=1}^{Q} \alpha^j(\boldsymbol{x})\boldsymbol{f}^j(\boldsymbol{x}) = \boldsymbol{c}(\boldsymbol{x})$$

Handling linear equality constraints

$$\sum_{j=1}^{Q} \alpha^j(\boldsymbol{x})\boldsymbol{f}^j(\boldsymbol{x}) = \boldsymbol{c}(\boldsymbol{x})$$

Principle of deductive approach

- Select arbitrary one output $\boldsymbol{f}^l$
- Build **unconstrained surrogates** $(\widehat{\boldsymbol{f}}^j, \boldsymbol{j} \neq \boldsymbol{l})$ on the remaining Q-1 outputs (independent or joint modeling)
- Deduce $\boldsymbol{f}^l$ prediction using constraint equation:

$$\widehat{\boldsymbol{f}}^l = \frac{\mathbf{1}}{\alpha^l(\boldsymbol{x})}\left(\boldsymbol{c}(\boldsymbol{x}) - \sum_{j\neq l} \alpha^j(\boldsymbol{x})\widehat{\boldsymbol{f}}^j(\boldsymbol{x})\right)$$

Handling linear equality constraints

$$\sum_{j=1}^{Q} \alpha^j(\boldsymbol{x}) \boldsymbol{f}^j(\boldsymbol{x}) = \boldsymbol{c}(\boldsymbol{x})$$

Principle of deductive approach

- Select arbitrary one output $\boldsymbol{f^l}$
- Build **unconstrained surrogates** $(\hat{\boldsymbol{f}}^{\boldsymbol{j}}, \boldsymbol{j} \neq \boldsymbol{l})$ on the remaining Q-1 outputs (independent or joint modeling)
- Deduce $\boldsymbol{f^l}$ prediction using constraint equation:

$$\hat{\boldsymbol{f}}^{l} = \frac{\mathbf{1}}{\alpha^l(\boldsymbol{x})}\left(\boldsymbol{c}(\boldsymbol{x}) - \sum_{\boldsymbol{j}\neq\boldsymbol{l}} \alpha^j(\boldsymbol{x}) \hat{\boldsymbol{f}}^{\boldsymbol{j}}(\boldsymbol{x})\right)$$

Parametrization approach[2] : Constrained GP

- Rewrite the linear constraint on f: $\mathcal{L}[f] = 0$, $\mathcal{L}$ linear operator
- Suppose that: $f(x) = \mathcal{G}_x[g]$
- Then we impose the constraint on the linear operator $\mathcal{G}_x$:

$$\boxed{\mathcal{L}[\mathcal{G}_x] = 0}$$

- Gaussian processes are closed under linear transformation

$$g \sim \mathcal{GP}(\mu_g(x), k_g(x, x'))$$

$$\mu_f(x) = \mathcal{G}_x[\mu_g], \qquad k_f = \mathcal{G}_x k_g \mathcal{G}_x^T$$

[2] Jidling, C., Wahlström, N., Wills, A., & Schön, T. B. (2017)

Constrained Gaussian Process regression

Given a linear constraint on f: $\mathcal{L}[f] = 0$, $\mathcal{L}$ linear operator

Parametrization approach[2] :

- Suppose that: $f(x) = \mathcal{G}_x[g]$
- Then we impose the constraint on the operator $\mathcal{G}_x$:

$$\boxed{\mathcal{L}[\mathcal{G}_x] = 0}$$

- Gaussian processes are closed under linear transformation

$$g \sim \mathcal{GP}(\mu_g(x), k_g(x, x'))$$

$$\mu_f(x) = \mathcal{G}_x[\mu_g], \qquad k_f = \mathcal{G}_x k_g \mathcal{G}_x^T$$

[2] Jidling, C., Wahlström, N., Wills, A., & Schön, T. B. (2017)

Constrained Gaussian Process regression

Given a linear constraint on f: $\mathcal{L}[f] = 0$, $\mathcal{L}$ linear operator

Parametrization approach[2] :

- Suppose that: $f(x) = \mathcal{G}_x[g]$
- Then we impose the constraint on the operator $\mathcal{G}_x$:

$$\boxed{\mathcal{L}[\mathcal{G}_x] = 0}$$

- Gaussian processes are closed under linear transformation

$$g \sim \mathcal{GP}(\mu_g(x), k_g(x, x'))$$

$$\mu_f(x) = \mathcal{G}_x[\mu_g], \qquad k_f = \mathcal{G}_x k_g \mathcal{G}_x^T$$

Illustration: $\mathcal{L}[f] = f_1 + f_2 = 0$

Constrained GP illustration

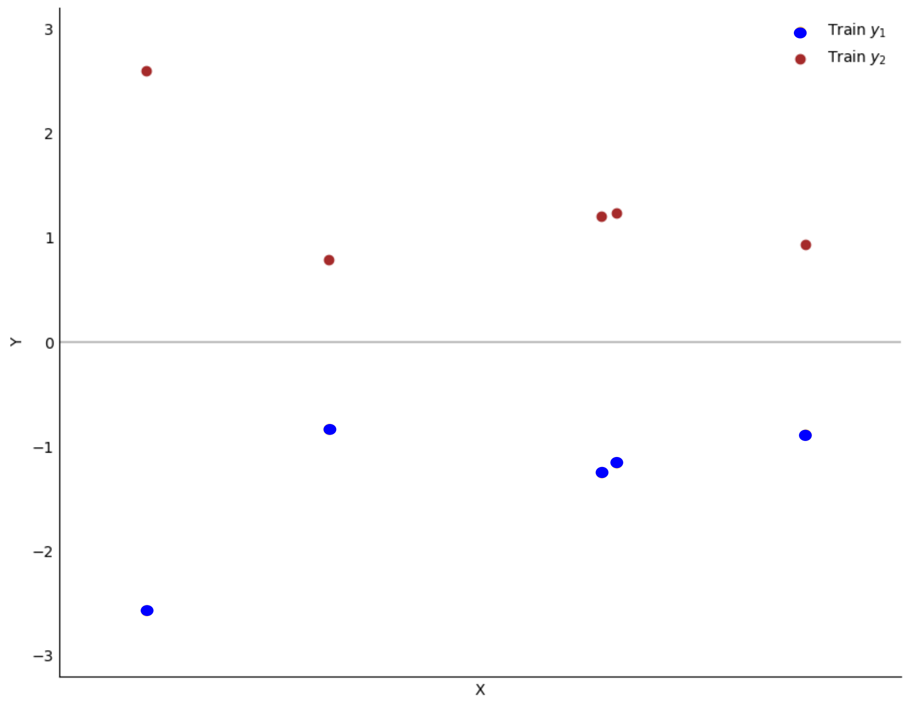

[2] Jidling, C., Wahlström, N., Wills, A., & Schön, T. B. (2017)

Constrained Gaussian Process regression

Given a linear constraint on f: $\mathcal{L}[f] = 0$, $\mathcal{L}$ linear operator

Parametrization approach[2] :

- Suppose that: $f(x) = \mathcal{G}_x[g]$
- Then we impose the constraint on the operator $\mathcal{G}_x$:

$$\mathcal{L}[\mathcal{G}_x] = 0$$

- Gaussian processes are closed under linear transformation

$$g \sim \mathcal{GP}(\mu_g(x), k_g(x, x'))$$

$$\mu_f(x) = \mathcal{G}_x[\mu_g], \qquad k_f = \mathcal{G}_x k_g \mathcal{G}_x^T$$

Illustration: $\mathcal{L}[f] = f_1 + f_2 = 0$

Constrained GP illustration

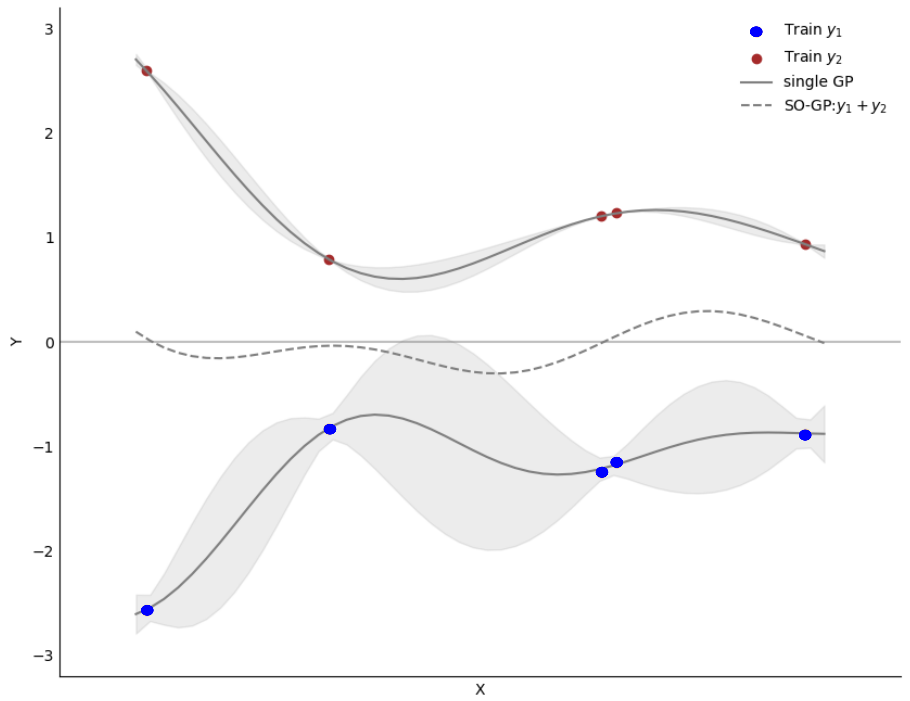

[2] Jidling, C., Wahlström, N., Wills, A., & Schön, T. B. (2017)

Constrained Gaussian Process regression

Given a linear constraint on f: $\mathcal{L}[f] = 0$, $\mathcal{L}$ linear operator

Parametrization approach[2] **:**

- Suppose that: $f(x) = \mathcal{G}_x[g]$
- Then we impose the constraint on the operator $\mathcal{G}_x$:

$$\mathcal{L}[\mathcal{G}_x] = 0$$

- Gaussian processes are closed under linear transformation

$$g \sim \mathcal{GP}(\mu_g(x), k_g(x, x'))$$

$$\mu_f(x) = \mathcal{G}_x[\mu_g], \qquad k_f = \mathcal{G}_x k_g \mathcal{G}_x^T$$

Illustration: $\mathcal{L}[f] = f_1 + f_2 = 0$

- $\mathcal{G}_x = [1, -1]$
- $\mu_f(x) = [\mu_g, -\mu_g]^T,\ k_f = \begin{bmatrix} 1 & -1 \\ -1 & 1 \end{bmatrix} k_g$

Constrained GP illustration

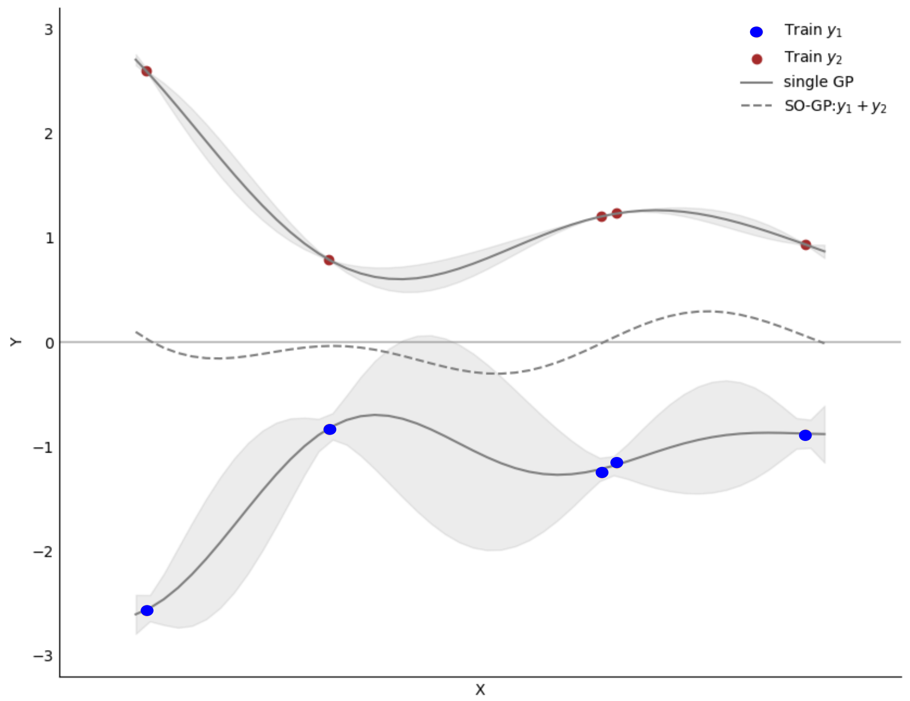

[2] Jidling, C., Wahlström, N., Wills, A., & Schön, T. B. (2017)

Constrained Gaussian Process regression

Given a linear constraint on f: $\mathcal{L}[f] = 0$, $\mathcal{L}$ linear operator

Parametrization approach[2] **:**

- Suppose that: $f(x) = \mathcal{G}_x[g]$
- Then we impose the constraint on the operator $\mathcal{G}_x$:

$$\boxed{\mathcal{L}[\mathcal{G}_x] = 0}$$

- Gaussian processes are closed under linear transformation

$$g \sim \mathcal{GP}(\mu_g(x), k_g(x, x'))$$

$$\mu_f(x) = \mathcal{G}_x[\mu_g], \qquad k_f = \mathcal{G}_x k_g \mathcal{G}_x^T$$

Illustration: $\mathcal{L}[f] = f_1 + f_2 = 0$

- $\mathcal{G}_x = [1, -1]$
- $\mu_f(x) = [\mu_g, -\mu_g]^T$, $k_f = \begin{bmatrix} 1 & -1 \\ -1 & 1 \end{bmatrix} k_g$

Constrained GP illustration

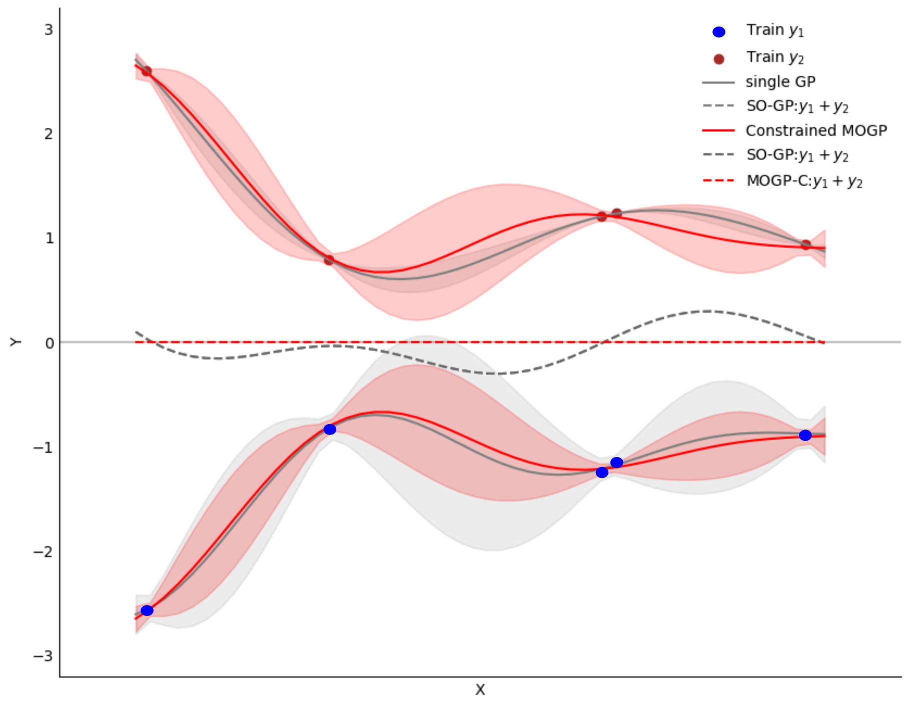

[2] Jidling, C., Wahlström, N., Wills, A., & Schön, T. B. (2017)

Comparison of deductive approaches and Constrained MOGP

Deductive approaches: LCM, Independent GP
Joint approach: Constrained MOGP

Analytical benchmark:

$D = 3, S = 1, Q = 3, P = 3$

- Normalized inputs $x \in \mathbb{R}^3$
- Normalized outputs

f^1 = Ishigami function
f^2 = Branin function
$f^3 = -f^1 - f^2$

Main findings

× **Heterogenous performances** in deduction-based methods, independent from the size of training set N

✓ Constrained MOGP achieves **better** or **comparable** predictive accuracy against best scenario of deductive approaches

Comparison of deductive approaches and Constrained MOGP

Deductive approaches: LCM, Independent GP
Joint approach: Constrained MOGP

Analytical benchmark:

$D = 3, S = 1, Q = 3, P = 3$

- Normalized inputs $x \in \mathbb{R}^3$
- Normalized outputs

f^1 = Ishigami function
f^2 = Branin function
$f^3 = -f^1 - f^2$

Main findings

× **Heterogenous performances** in deduction-based methods, independent from the size of training set N

✓ Constrained MOGP achieves **better** or **comparable** predictive accuracy against best scenario of deductive approaches

Problem: $\mathcal{O}(N^3P^3)$ complexity !

Need to be combined with a dimensionality reduction techniques,

but how, and which techniques ?

PCA for multi-field data[3]

Computer code output:

k^{th} field
1 sample

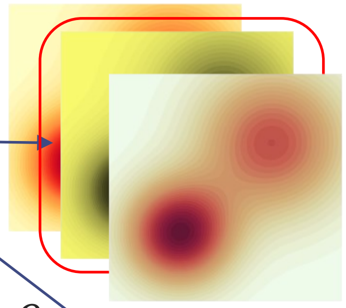

Q

matrix representation

$$\boldsymbol{Y_k} = \begin{bmatrix} y^k_{1,1} & y^k_{1,S} \\ & \\ & \end{bmatrix}$$

PCA for multi-field data[3]

Computer code output:

k^{th} field
N samples

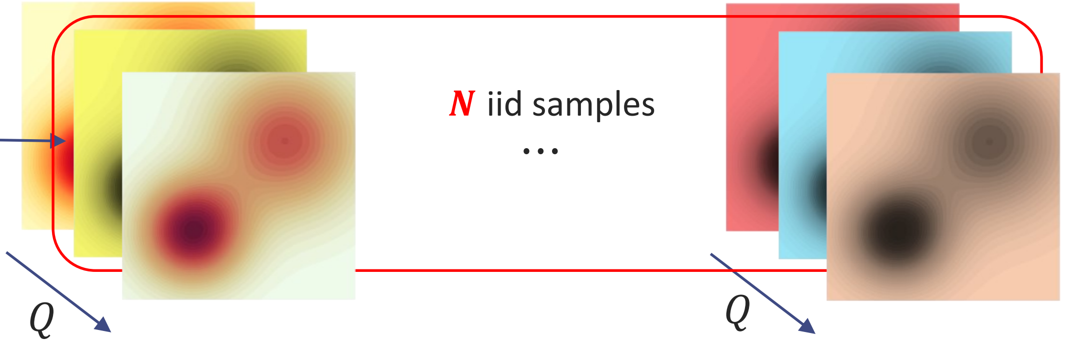

matrix representation

$$\boldsymbol{Y_k} = \begin{bmatrix} y^k_{1,1} & & y^k_{1,S} \\ \vdots & \cdots & \vdots \\ y^k_{N,1} & & y^k_{N,S} \end{bmatrix}$$

PCA for multi-field data[3]

Computer code output:

k^{th} field
N samples

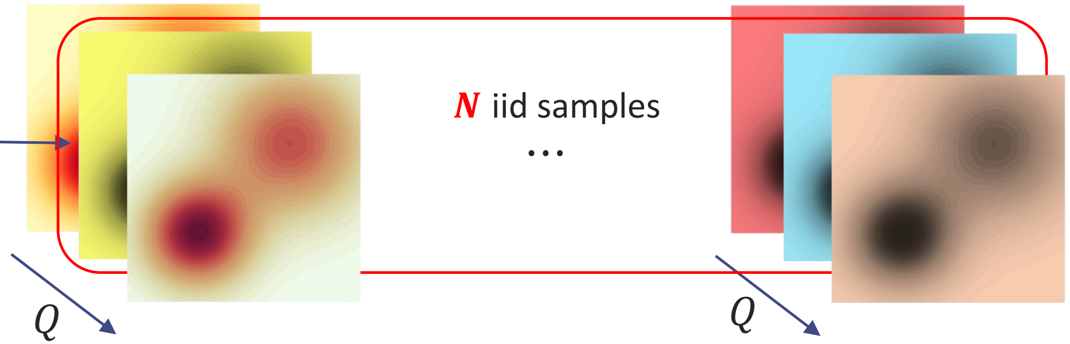

matrix representation

$$\boldsymbol{Y_k} = \begin{bmatrix} y^k_{1,1} & & y^k_{1,S} \\ \vdots & \cdots & \vdots \\ y^k_{N,1} & & y^k_{N,S} \end{bmatrix}$$

- There is Q data matrices for Q physical fields: $\boldsymbol{Y_1}, \dots, \boldsymbol{Y_Q}$ $\Longrightarrow$ How can we reduce their dimension $\boldsymbol{S}$?

PCA for multi-field data[3]

Computer code output:

k^{th} field
N samples

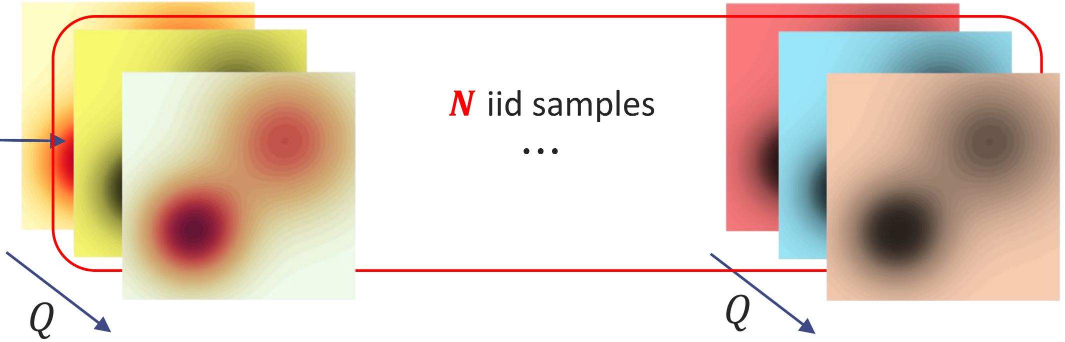

matrix representation

$$Y_k = \begin{bmatrix} y^k_{1,1} & & y^k_{1,S} \\ \vdots & \dots & \vdots \\ y^k_{N,1} & & y^k_{N,S} \end{bmatrix}$$

- There is Q data matrices for Q physical fields: $Y_1, \dots, Y_Q$ $\Longrightarrow$ How can we reduce their dimension S ?

	Data matrix	SVD	Cov matrix	Rank m Projector	Reconstruction error
Field-wise PCA	$Y_k \in \mathbb{R}^{N\times S}$	$Y_k = U_k D_k V_k^T$	$\Sigma_k = \frac{1}{N} Y_k^T Y_k$, $K_k = \frac{1}{S} Y_k Y_k^T$	$P_{k,m} = V_{k,m} V_{k,m}^T$	$\varepsilon^{field}_{k,m} = \Vert Y_k - Y_k P_{k,m} \Vert_F$
Col-wise PCA	$Y_{col} = [Y_1, \cdots, Y_Q] \in \mathbb{R}^{N\times QS}$	$Y_{col} = U_{col} D_{col} V_{col}$	$K_{col} = \frac{1}{N} Y_{col} Y_{col}^T$	$\Pi_{col,m} = U_{col} U_{col}^T$	$\varepsilon^{col}_{m,k} = \Vert Y_k - \Pi_{col,m} Y_k \Vert_F$
Row-wise PCA	$Y_{row} = \begin{bmatrix} Y_1 \\ \vdots \\ Y_k \\ \vdots \\ Y_Q \end{bmatrix} \in \mathbb{R}^{QN\times S}$	$Y_{row} = U_{row} D_{row} V_{row}$	$\Sigma_{row} = \frac{1}{QN} Y_{row}^T Y_{row}$	$P_{row,m} = V_{row,m} V_{row,m}^T$	$\varepsilon^{row}_{m,k} = \Vert Y_k - Y_k P_{row,m} \Vert_F$

PCA for multi-field data[3]

Computer code output:

k^{th} field
N samples

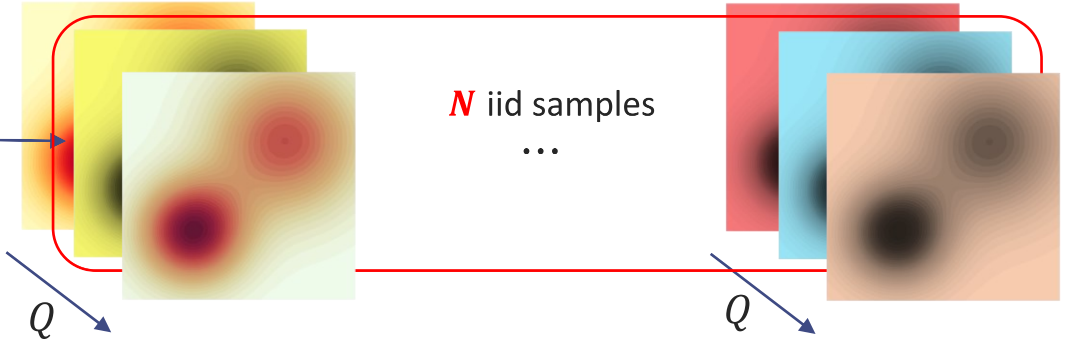

matrix representation

$$\boldsymbol{Y_k} = \begin{bmatrix} y^k_{1,1} & & y^k_{1,S} \\ \vdots & \dots & \vdots \\ y^k_{N,1} & & y^k_{N,S} \end{bmatrix}$$

- There is Q data matrices for Q physical fields: $\boldsymbol{Y_1}, \dots, \boldsymbol{Y_Q}$ $\Longrightarrow$ How can we reduce their dimension $\boldsymbol{S}$?

	Data matrix	SVD	Cov matrix	Rank m Projector	Reconstruction error
Field-wise PCA	$\boldsymbol{Y_k} \in \mathbb{R}^{N \times \boldsymbol{S}}$	$\boldsymbol{Y_k} = \boldsymbol{U_k D_k V_k^T}$	$\boldsymbol{\Sigma_k} = \frac{1}{N}\boldsymbol{Y_k^T Y_k}$, $\boldsymbol{K_k} = \frac{1}{S}\boldsymbol{Y_k Y_k^T}$	$\boldsymbol{P_{k,m}} = \boldsymbol{V_{k,m} V_{k,m}^T}$	$\mathcal{E}^{field}_{k,m} = \Vert \boldsymbol{Y_k} - \boldsymbol{Y_k P_{k,m}} \Vert_F$
Col-wise PCA	$\boldsymbol{Y_{col}} = [\boldsymbol{Y_1}, \cdots, \boldsymbol{Y_Q}] \in \mathbb{R}^{N \times \boldsymbol{QS}}$	$\boldsymbol{Y_{col}} = \boldsymbol{U_{col} D_{col} V_{col}}$	$\boldsymbol{K_{col}} = \frac{1}{N}\boldsymbol{Y_{col} Y_{col}^T}$	$\boldsymbol{\Pi_{col,m}} = \boldsymbol{U_{col} U_{col}^T}$	$\mathcal{E}^{col}_{m,k} = \Vert \boldsymbol{Y_k} - \boldsymbol{\Pi_{col,m} Y_k} \Vert_F$
Row-wise PCA	$\boldsymbol{Y_{row}} = \begin{bmatrix} \boldsymbol{Y_1} \\ \vdots \\ \boldsymbol{Y_k} \\ \vdots \\ \boldsymbol{Y_Q} \end{bmatrix} \in \mathbb{R}^{QN \times \boldsymbol{S}}$	$\boldsymbol{Y_{row}} = \boldsymbol{U_{row} D_{row} V_{row}}$	$\boldsymbol{\Sigma_{row}} = \frac{1}{QN}\boldsymbol{Y_{row}^T Y_{row}}$	$\boldsymbol{P_{row,m}} = \boldsymbol{V_{row,m} V_{row,m}^T}$	$\mathcal{E}^{row}_{m,k} = \Vert \boldsymbol{Y_k} - \boldsymbol{Y_k P_{row,m}} \Vert_F$

☛ **Which approach is optimal and well suited for a combination with Constrained MOGP ?**

Theoretical analysis and comparison

- **Row-wise PCA vs field-wise PCA**

Theorem 1: (Row-wise excess error bound)

Let $\delta_k = \lambda_m^k - \lambda_{m+1}^k$, where λ_m^k denotes the m-th eigenvalue of $\boldsymbol{\Sigma}_k$ in decreasing order. If $\delta_k > 0$, then the row-wise excess error $\Delta\mathcal{E}_{k,m}^{row} = \mathcal{E}_{k,m}^{field} - \mathcal{E}_{k,m}^{row}$ of the k-th field is directly bounded by

$$\Delta\mathcal{E}_{k,m}^{row} \leq \frac{2n\sqrt{2} \parallel \boldsymbol{\Sigma}_k \parallel_F}{\delta_k} \min\left(\frac{\sqrt{m}}{Q}\sum_{j=1}^{Q} \parallel \boldsymbol{\Sigma}_j - \boldsymbol{\Sigma}_k \parallel_{op}, \frac{1}{Q}\sum_{j=1}^{Q} \parallel \boldsymbol{\Sigma}_j - \boldsymbol{\Sigma}_k \parallel_F\right)$$

- **Col-wise PCA vs field-wise PCA**

Theorem 2: (Col-wise excess error bound)

Let $\delta_k = \lambda_m^k - \lambda_{m+1}^k$. If $\delta_k > 0$, then the col-wise excess error $\Delta\mathcal{E}_{k,m}^{col} = \mathcal{E}_{k,m}^{field} - \mathcal{E}_{k,m}^{col}$ of the k-th field is directly bounded by the distance between Gram matrices:

$$\Delta\mathcal{E}_{k,m}^{col} \leq \frac{2S\sqrt{2} \parallel \boldsymbol{K}_k \parallel_F}{\delta_k} \min\left(\frac{\sqrt{m}}{Q}\sum_{j=1}^{Q} \parallel \boldsymbol{K}_j - \boldsymbol{K}_k \parallel_{op}, \frac{1}{Q}\sum_{j=1}^{Q} \parallel \boldsymbol{K}_j - \boldsymbol{K}_k \parallel_F\right)$$

☛ **Theorem 1 & 2 bounds guarantee bounded excess error whenever fields exhibit structural similarities, providing a theoretical justification of using multi-field PCA over field-wise when these similarities hold**

Theoretical analysis and comparison

- **Row-wise PCA vs col-wise PCA**

Theorem 3: (Col-wise vs row-wise performance)

Let $\Lambda_{row,m} = nQ\sum_{j=1}^{m}\lambda_m^{\Sigma_{row}}$, $\Lambda_{col,m} = QS\sum_{j=1}^{m}\lambda_m^{K_{col}}$. The difference between the reconstruction error of the column-wise and row-wise approaches at rank m is exactly :

$$\mathcal{E}_{k,m}^{col} - \mathcal{E}_{k,m}^{row} = \mathrm{Tr}\left(D_{row,m}^2\right) - \mathrm{Tr}\left(D_{col,m}^2\right) = \Lambda_{row,m} - \Lambda_{col,m}$$

☛ **Neither strategy is intrinsically superior between row-wise and col-wise and the theorem gives an exact dominance criterion**

❑ Constrained fields case:

- ✗ Field wise and column wise approaches fail to guarantee constraint satisfaction in reconstruction
- ✗ To satisfy linear constraints, they must be used with deductive approaches principle
- ✓ **Row-wise approach preserves linear constraints both in latent space, and in the reconstructed fields**
  - ☛ We propose to combine **row-wise PCA + Constrained MOGP** to solve our initial problem
- ✓ We have **numerically validated** our theoretical results on an analytical benchmark based on **Lotka-Volterra** model

Metamodel for the turbulent Reynolds stress tensor

- **Context**: Uncertainty propagation study in RANS modeling
- Turbulence closure model: standard $k - \varepsilon$
- **Inputs**: closure parameters of the standard $k - \varepsilon$ turbulence model

$$\boldsymbol{x} = \left(C_\mu, \sigma_k, \sigma_\varepsilon, C_{\varepsilon_1}, C_{\varepsilon_2}\right)$$

- **Output**: Reynolds stress tensor $\tau_{ij} = \overline{u_i' u_j'}$ and the turbulent kinetic energy k

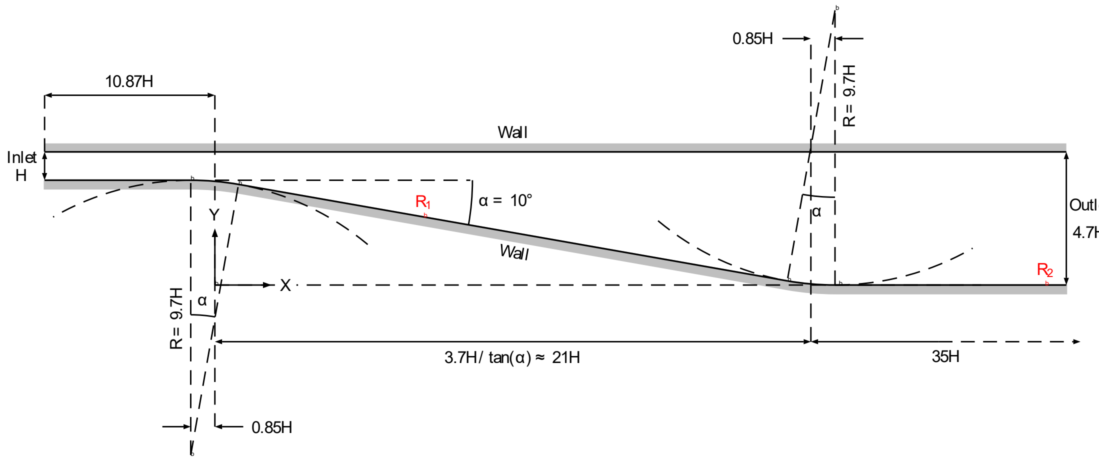

Figure: Scheme of the experiment carried out in Buice and Eaton, 2000. The wall of the channel are defined by straight lines and circular arcs of centers O_1 and O_2

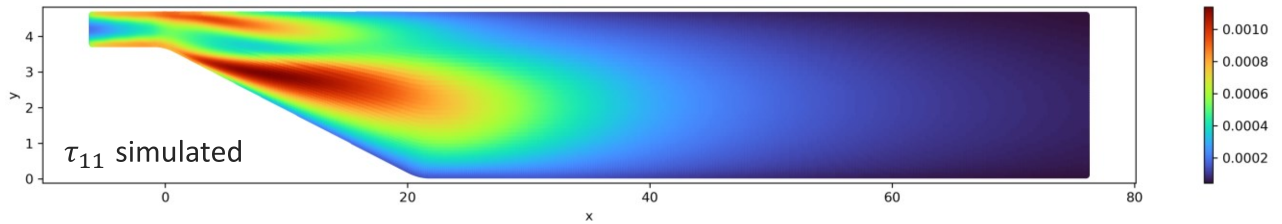

Metamodel for the turbulent Reynolds stress tensor

- **Context**: Uncertainty propagation study in RANS modeling
- Turbulence closure model: standard $k - \varepsilon$
- **Inputs**: closure parameters of the standard $k - \varepsilon$ turbulence model

$$\boldsymbol{x} = \left(C_\mu, \sigma_k, \sigma_\varepsilon, C_{\varepsilon_1}, C_{\varepsilon_2}\right)$$

- **Output**: Reynolds stress tensor $\tau_{ij} = \overline{u_i' u_j'}$ and the turbulent kinetic energy k
- The incompressibility condition is translated by:

$$\boldsymbol{\tau_{11} + \tau_{22} - \frac{4}{3} k = 0}$$

Datasets generation details:

- Mesh composed of 200 000 triangular elements
- CEA/DES CFD solver TrioCFD
- Reynolds number = 18000
- N_{train} = 50 and $N_{test} = 100$

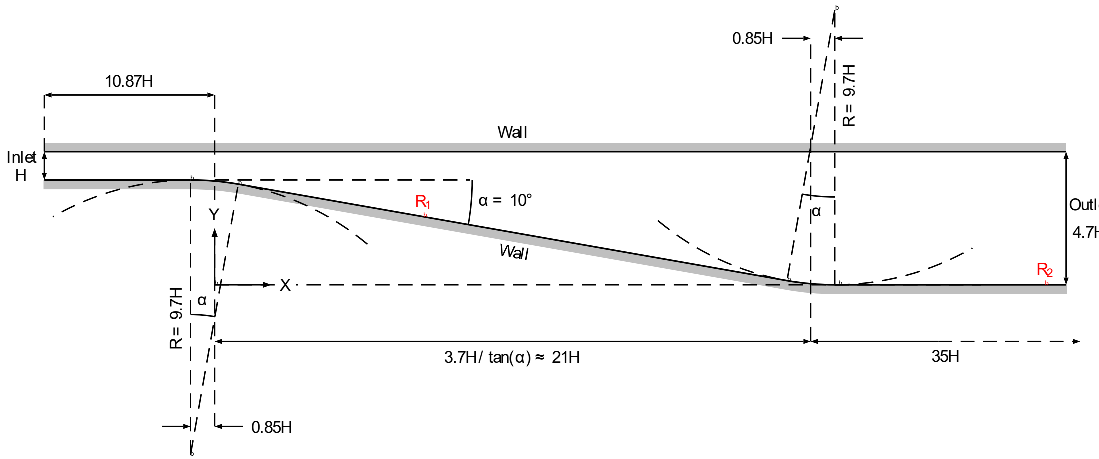

Figure: Scheme of the experiment carried out in Buice and Eaton, 2000. The wall of the channel are defined by straight lines and circular arcs of centers O_1 and O_2

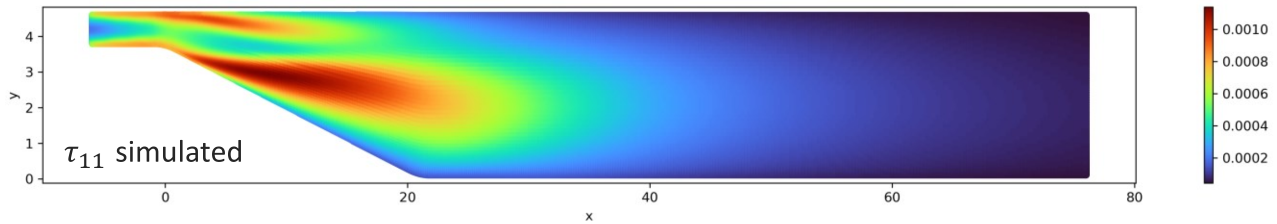

RRMSE result on the LEVM Reynolds stress tensor

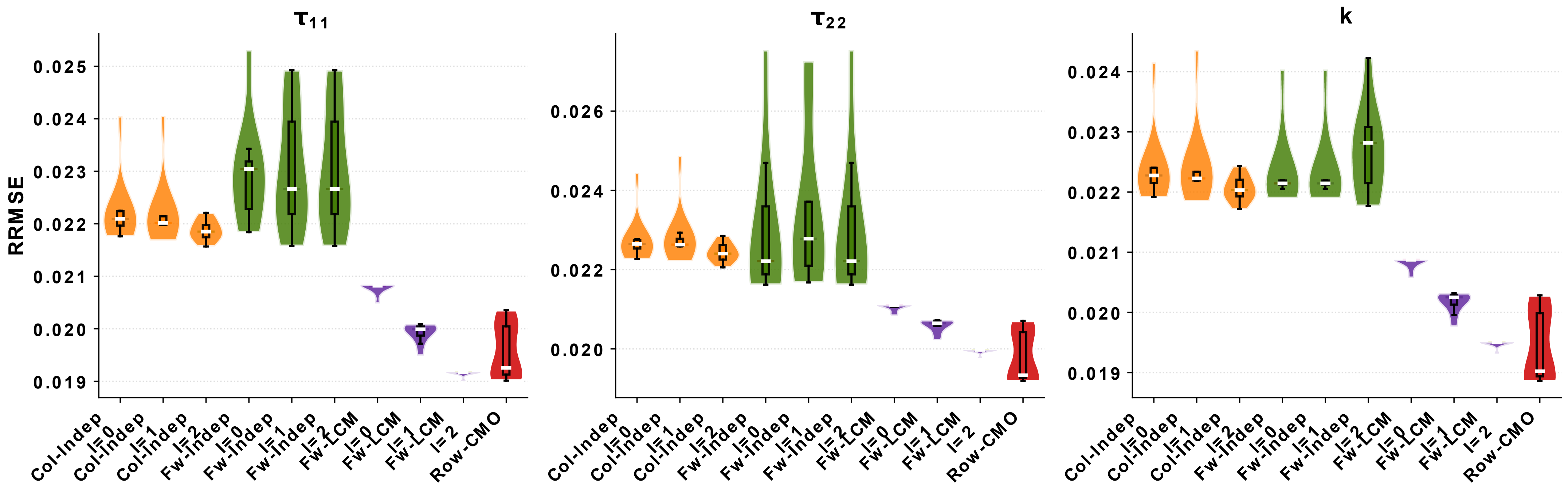

Fig: Final RRMSE (median ±std) with m=8 latent dimension for each method. Our method Row-CMO against 3 deductive alternatives

RRMSE result on the LEVM Reynolds stress tensor

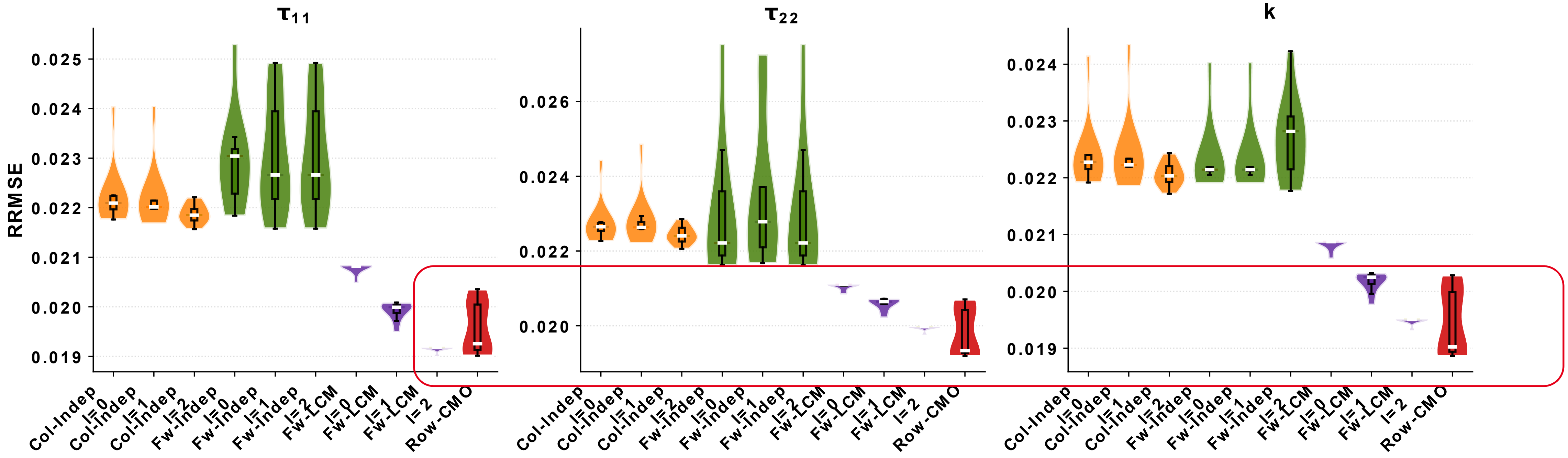

Fig: Final RRMSE (median ±std) with m=8 latent dimension for each method. Our method Row-CMO against 3 deductive alternatives

- **Final RRMSE reveals that our method ends up outperforming alternatives and achieves the lowest RRMSE on all three outputs.**
- **Deductive approaches yield varying results across variants: this confirms their inherent instability**

Prediction and uncertainty illustration

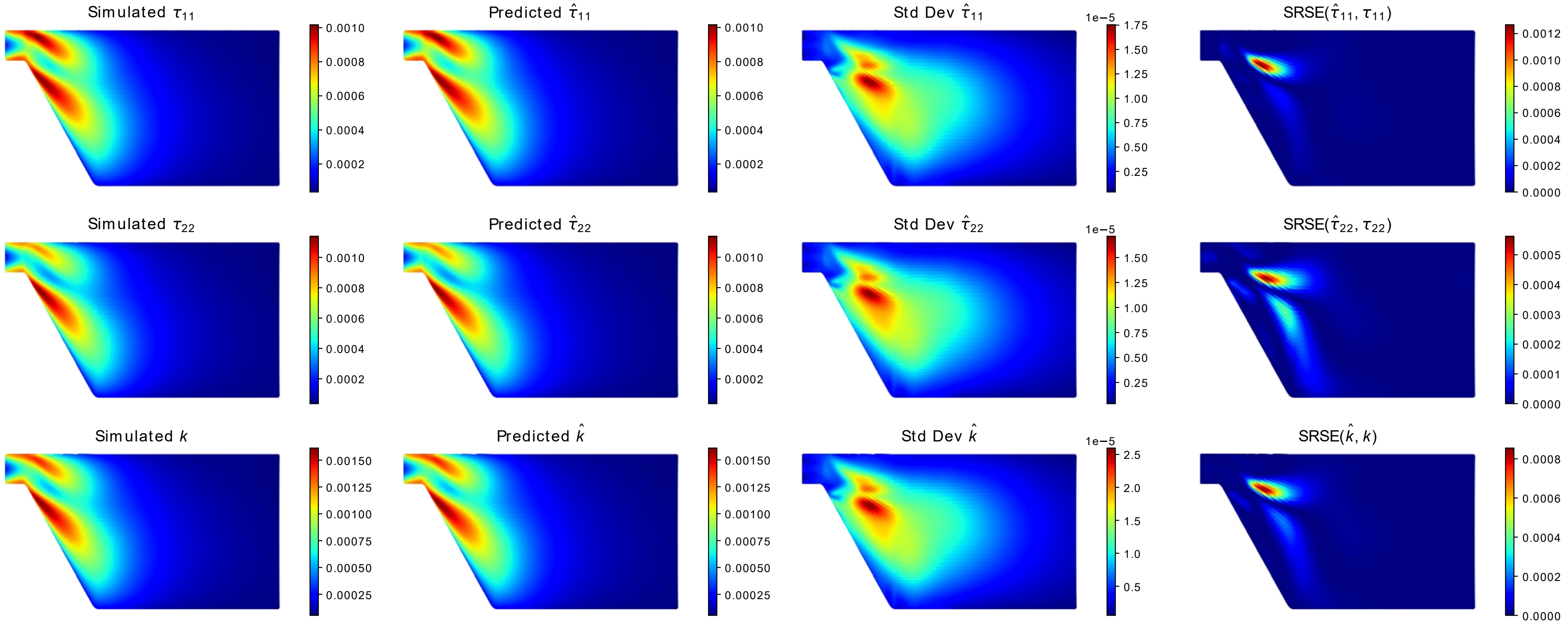

Fig: Row-wise PCA-Constrained MOGP predictions of the CFD test case for a representative test input (with m=8)

The model accurately captures the spatial structure. Error and uncertainty are concentrated in the recirculation zone of the diffuser.

Conclusion

- ✓ We introduce a constrained GP framework for for high dimensional fields that combines row-wise PCA with joint modeling to efficiently handle linearly constrained physical fields

Conclusion

- ✓ We introduce a constrained GP framework for for high dimensional fields that combines row-wise PCA with joint modeling to efficiently handle linearly constrained physical fields

- ✓ We provide a theoretical analysis that quantifies when this PCA strategy remains competitive with standard approaches, beyond its key advantage of full compatibility with constrained MOGP

Conclusion

- ✓ We introduce a constrained GP framework for for high dimensional fields that combines row-wise PCA with joint modeling to efficiently handle linearly constrained physical fields

- ✓ We provide a theoretical analysis that quantifies when this PCA strategy remains competitive with standard approaches, beyond its key advantage of full compatibility with constrained MOGP

- ✓ Through benchmark, we demonstrate the robustness of joint modeling compared to deductive approaches which can exhibit heterogenous performances

Conclusion

- ✓ We introduce a constrained GP framework for for high dimensional fields that combines row-wise PCA with joint modeling to efficiently handle linearly constrained physical fields
- ✓ We provide a theoretical analysis that quantifies when this PCA strategy remains competitive with standard approaches, beyond its key advantage of full compatibility with constrained MOGP
- ✓ Through benchmark, we demonstrate the robustness of joint modeling compared to deductive approaches which can exhibit heterogenous performances
- ✓ Finally, we validate the practical relevance of our approach on an industrial CFD case, highlighting clear benefits in data-scarce settings

Conclusion

- ✓ We introduce a constrained GP framework for for high dimensional fields that combines row-wise PCA with joint modeling to efficiently handle linearly constrained physical fields
- ✓ We provide a theoretical analysis that quantifies when this PCA strategy remains competitive with standard approaches, beyond its key advantage of full compatibility with constrained MOGP
- ✓ Through benchmark, we demonstrate the robustness of joint modeling compared to deductive approaches which can exhibit heterogenous performances
- ✓ Finally, we validate the practical relevance of our approach on an industrial CFD case, highlighting clear benefits in data-scarce settings

Preprint available here =>

References

[1] Alvarez, M. A., Rosasco, L., & Lawrence, N. D. (2012). Kernels for vector-valued functions: A review. Foundations and Trends® in Machine Learning.

[2] Jidling, C., Wahlström, N., Wills, A., & Schön, T. B. (2017). Linearly constrained Gaussian processes. Advances in neural information processing systems.

[3] R. W. Preisendorfer and C. D. Mobley. (1988). Principal component analysis in meteorology and oceanography. Elsevier.

[4] Carl U. Buice and John K. Eaton. Experimental investigation of flow through an asymmetric plane diffuser: (data bank contribution)1. Journal of fluids Engineering, 122(2):433-435, 01 200. doi: 10.1115/1.483278.

Acknowledgments:

This work has been funded by the French *Agence Nationale de la Recherche* ExaMA project, under the France 2030 initiative, with reference ANR-22-EXNU-0002.

Thanks !

Any questions ?

Preprint link !

PROGRAMME DE RECHERCHE

NUMÉRIQUE POUR L'EXASCALE

Comparison of deductive approaches and Constrained MOGP

Analytical benchmark:

$D = 3, S = 1, Q = 3, P = 3$

- Normalized inputs $x \in \mathbb{R}^3$
- Normalized outputs

f^1 = Ishigami function
f^2 = Branin function
$f^3 = -f^1 - f^2$

Deductive approaches: LCM, Independent GP
Joint approach: Constrained MOGP

Comparison of deductive approaches and Constrained MOGP

RMSE of the predictive distribution of f^2: Violin plots across 200 train/test splits.

Analytical benchmark:

$D = 3, S = 1, Q = 3, P = 3$

- Normalized inputs $x \in \mathbb{R}^3$
- Normalized outputs

f^1 = Ishigami function
f^2 = Branin function
$f^3 = -f^1 - f^2$

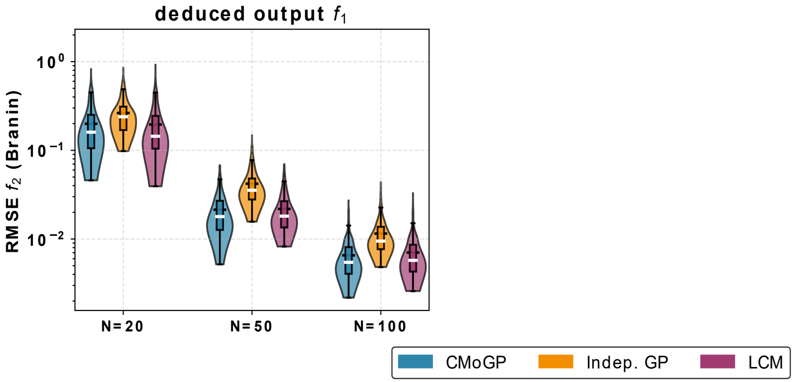

Deductive approaches: LCM, Independent GP
Joint approach: Constrained MOGP

Comparison of deductive approaches and Constrained MOGP

RMSE of the predictive distribution of f^2: Violin plots across 200 train/test splits.

Analytical benchmark:

$D = 3, S = 1, Q = 3, P = 3$

- Normalized inputs $x \in \mathbb{R}^3$
- Normalized outputs

f^1 = Ishigami function
f^2 = Branin function
$f^3 = -f^1 - f^2$

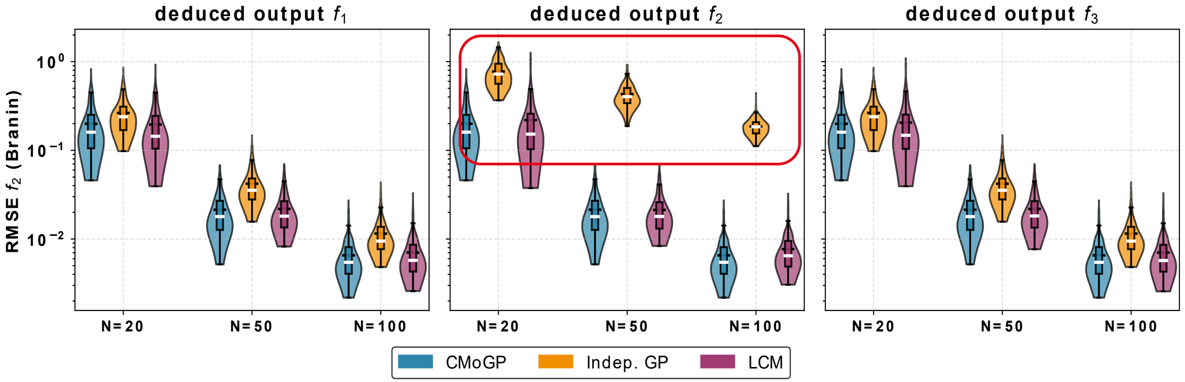

Deductive approaches: LCM, Independent GP
Joint approach: Constrained MOGP

Comparison of deductive approaches and Constrained MOGP

Analytical benchmark:

$D = 3, S = 1, Q = 3, P = 3$

- Normalized inputs $x \in \mathbb{R}^3$
- Normalized outputs

f^1 = Ishigami function
f^2 = Branin function
$f^3 = -f^1 - f^2$

Deductive approaches: LCM, Independent GP
Joint approach: Constrained MOGP

RMSE of the predictive distribution of f^2: Violin plots across 200 train/test splits.

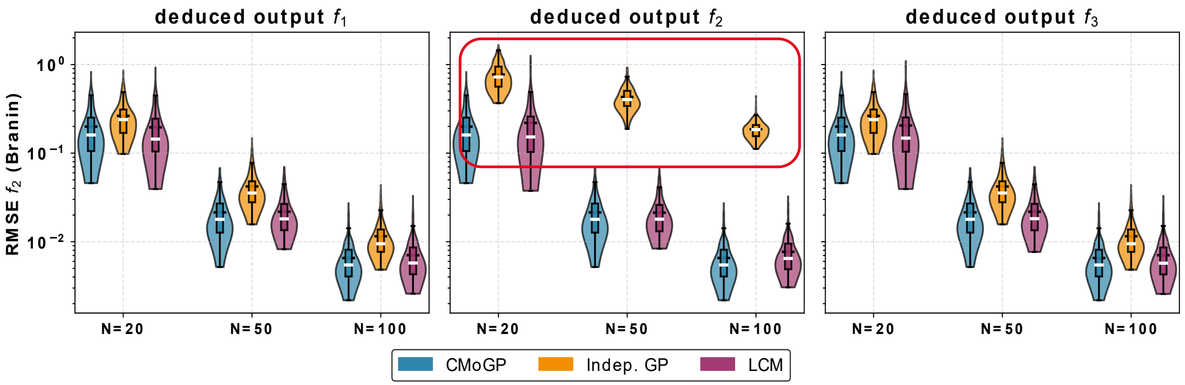

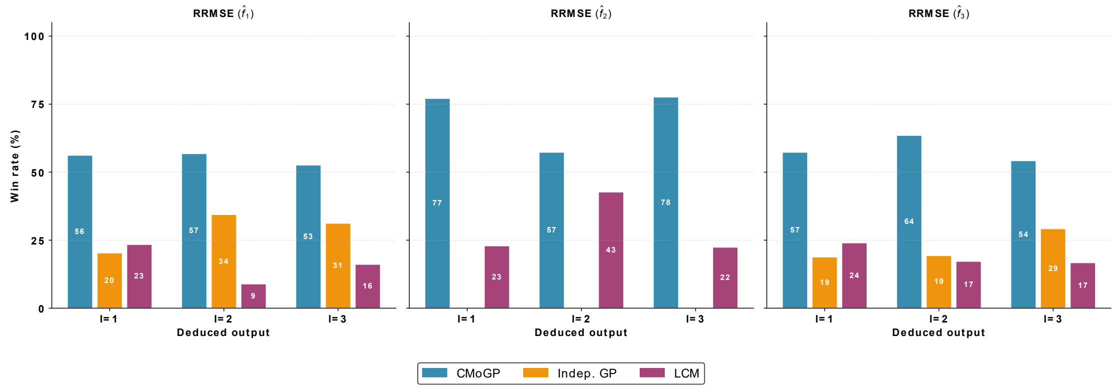

Win rate (%) of each method on the RMSE of each output (f^1, f^2, f^3) across all deduction scenarios with N=50.

Comparison of deductive approaches and Constrained MOGP

Analytical benchmark:

$D = 3, S = 1, Q = 3, P = 3$

- Normalized inputs $x \in \mathbb{R}^3$
- Normalized outputs

$f^1 =$ Ishigami function
$f^2 =$ Branin function
$f^3 = -f^1 - f^2$

Deductive approaches: LCM, Independent GP
Joint approach: Constrained MOGP

× **Heterogenous performances** in deduction-based methods, independent from the size of training set N
✓ Constrained MOGP achieves **better** or **comparable** predictive accuracy against best scenario of deductive approaches

RMSE of the predictive distribution of f^2: Violin plots across 200 train/test splits.

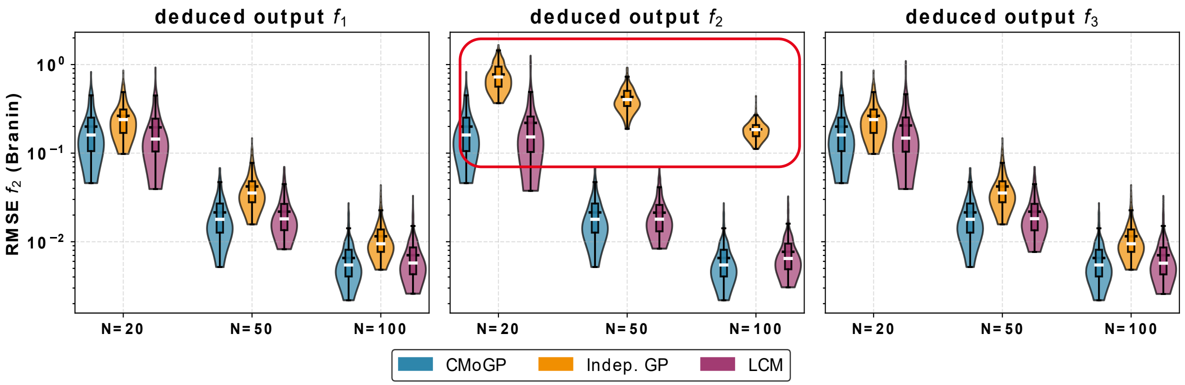

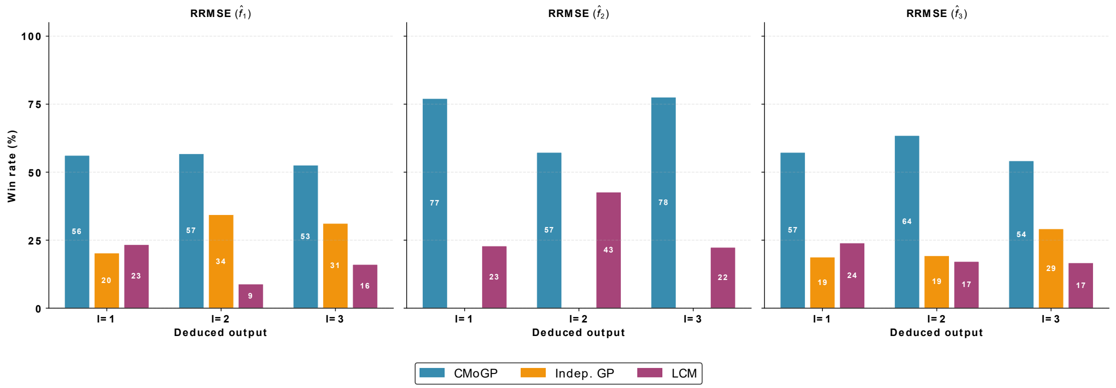

Win rate (%) of each method on the RMSE of each output (f^1, f^2, f^3) across all deduction scenarios with N=50.

Comparison of deductive approaches and Constrained MOGP

Analytical benchmark:

$D = 3, S = 1, Q = 3, P = 3$

- Normalized inputs $x \in \mathbb{R}^3$
- Normalized outputs

f^1 = Ishigami function
f^2 = Branin function
$f^3 = -f^1 - f^2$

Deductive approaches: LCM, Independent GP
Joint approach: Constrained MOGP

× **Heterogenous performances** in deduction-based methods, independent from the size of training set N

✓ Constrained MOGP achieves **better** or **comparable** predictive accuracy against best scenario of deductive approaches

Problem: $\mathcal{O}(N^3P^3)$ complexity !

Need to be combined with a dimensionality reduction techniques,

but how, and which techniques ?

RMSE of the predictive distribution of f^2: Violin plots across 200 train/test splits.

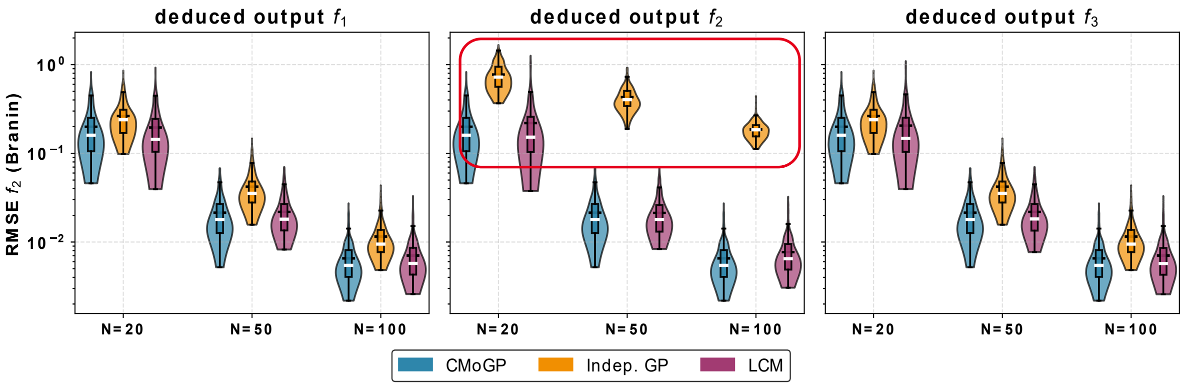

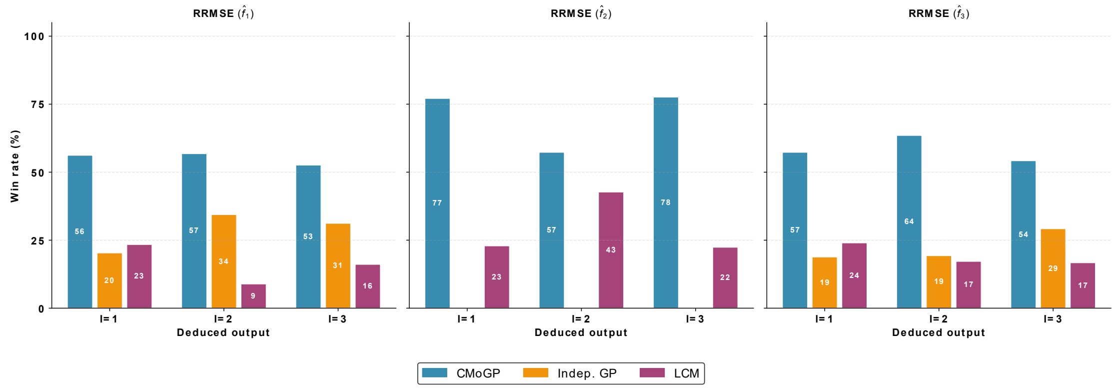

Win rate (%) of each method on the RMSE of each output (f^1, f^2, f^3) across all deduction scenarios with N=50.

Metamodel for population dynamics

- **Lotka-Volterra equations:**

p: prey density population
q: predator density population

$$\begin{cases} p'(t) = ap(t) - bp(t)q(t) \\ q'(t) = -cq(t) + dp(t)q(t) \end{cases} \quad (1)$$

$r(t) = \log(q(t)),\ s(t) = \log(p(t))$

- **Analytical benchmark configuration:**

$D = 2, S = 400, Q = 4\ , N_{test} = 100,\ \ b \in [0.37, 0.40],\ \ d \in [0.0, 0.06]$

- **Metamodeling problem:**

Inputs: $x = (b, d)$,
Outputs: $p(t), q(t), r(t), s(t)$
Constraint equation:

$$\boldsymbol{dp(t) - cs(t) + bq(t) - ar(t) = C_0}$$

Metamodel for population dynamics

- **Lotka-Volterra equations:**

p: prey density population

q: predator density population

$$\begin{cases} p'(t) = ap(t) - bp(t)q(t) \\ q'(t) = -cq(t) + dp(t)q(t) \end{cases} \quad (1)$$

$r(t) = \log(q(t)),\ s(t) = \log(p(t))$

- **Analytical benchmark configuration:**

$D = 2, S = 400, Q = 4\ , N_{test} = 100,\ \ b \in [0.37, 0.40],\ \ d \in [0.0, 0.06]$

- **Metamodeling problem:**

Inputs: $x = (b, d)$,

Outputs: $p(t), q(t), r(t), s(t)$

Constraint equation:

$$\boldsymbol{dp(t) - cs(t) + bq(t) - ar(t) = C_0}$$

Our model:

- Row-CMO = Row-wise PCA
  + CMoGP

Deductive approaches:

- Col-Indep = Column-wise PCA
  + Independent GP
- Fw-Indep = Field-wise PCA
  + Independent GP
- Fw-LCM: Field-wise PCA
  + LCM

l : Deduced output indices

Metamodel for population dynamics

- **Lotka-Volterra equations:**

p: prey density population
q: predator density population

$$\begin{cases} p'(t) = ap(t) - bp(t)q(t) \\ q'(t) = -cq(t) + dp(t)q(t) \end{cases} \quad (1)$$

$r(t) = \log\big(q(t)\big),\ s(t) = \log(p(t))$

- **Analytical benchmark configuration:**

$D = 2, S = 400, Q = 4\ , N_{test} = 100,\ b \in [0.37{,}0.40],\ d \in [0.0, 0.06]$

- **Metamodeling problem:**

Inputs: $x = (b, d)$,
Outputs: $p(t), q(t), r(t), s(t)$
Constraint equation:

$$\boldsymbol{dp(t) \ - cs(t) + bq(t) - ar(t) = C_0}$$

Our model:
- Row-CMO = Row-wise PCA + CMoGP

Deductive approaches:
- Col-Indep = Column-wise PCA + Independent GP
- Fw-Indep = Field-wise PCA + Independent GP
- Fw-LCM: Field-wise PCA + LCM

l : Deduced output indices

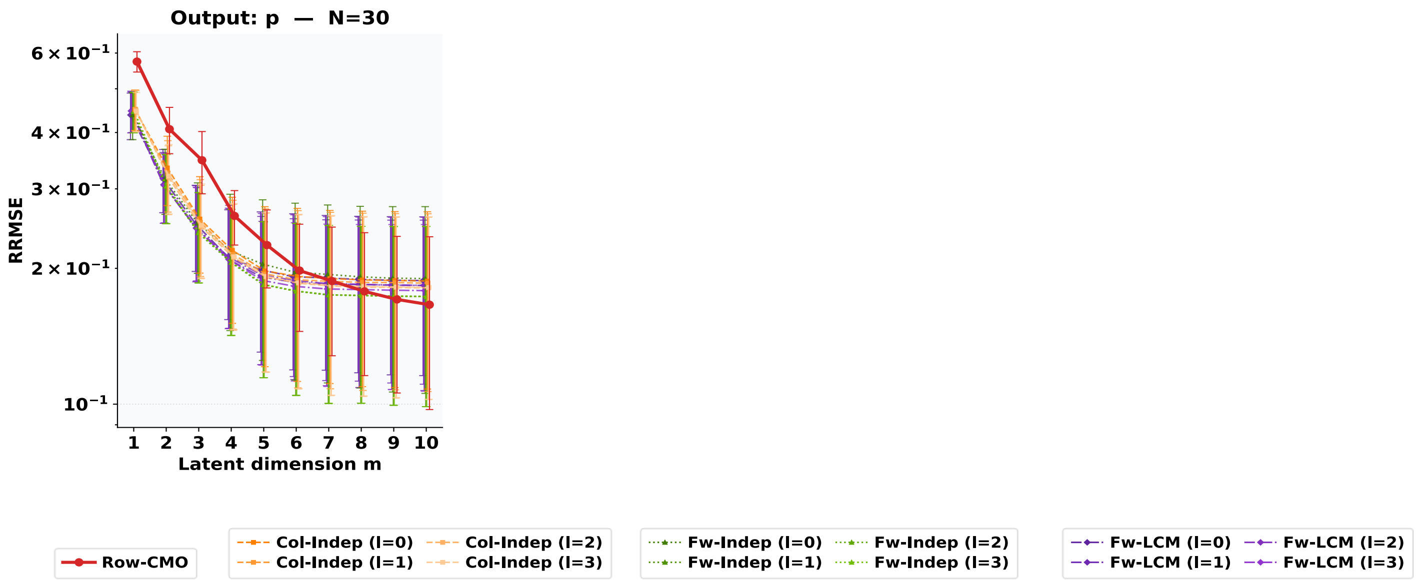

Fig: RRMSE (mean$\pm$std) on output p for all methods. **Beyond m=4, Row-CMO surpasses all alternative at higher latent dimensions**

Metamodel for population dynamics

- **Lotka-Volterra equations:**

p: prey density population
q: predator density population

$$\begin{cases} p'(t) = ap(t) - bp(t)q(t) \\ q'(t) = -cq(t) + dp(t)q(t) \end{cases} \quad (1)$$

$r(t) = \log(q(t)),\ s(t) = \log(p(t))$

- **Analytical benchmark configuration:**

$D = 2, S = 400, Q = 4\ , N_{test} = 100,\ \ b \in [0.37, 0.40],\ \ d \in [0.0, 0.06]$

- **Metamodeling problem:**

Inputs: $x = (b, d)$,
Outputs: $p(t), q(t), r(t), s(t)$
Constraint equation:

$$\boldsymbol{dp(t) \ - cs(t) + bq(t) - ar(t) = C_0}$$

Our model:

- Row-CMO = Row-wise PCA + CMoGP

Deductive approaches:

- Col-Indep = Column-wise PCA + Independent GP
- Fw-Indep = Field-wise PCA + Independent GP
- Fw-LCM: Field-wise PCA + LCM

l : Deduced output indices

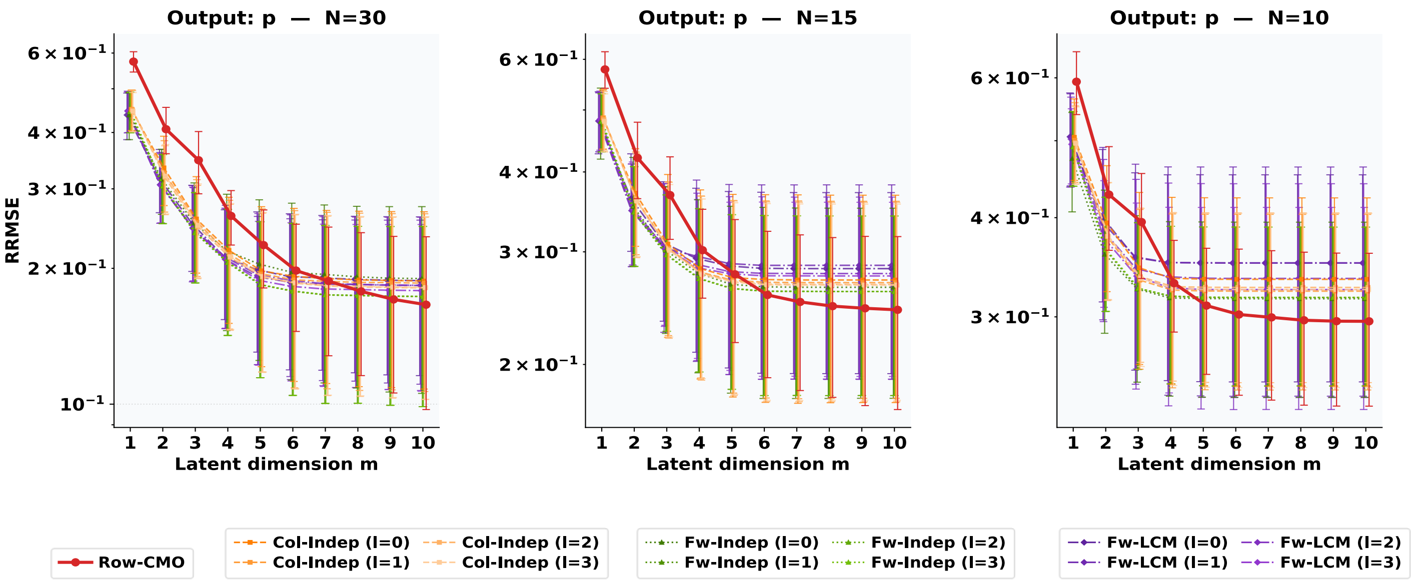

Fig: RRMSE (mean±std) on output p for all methods. **Beyond m=4, Row-CMO surpasses all alternative at higher latent dimensions**

Metamodel for the turbulent Reynolds stress tensor

- **Context**: Uncertainty propagation study in RANS modeling
- Turbulence closure model: standard $k-\varepsilon$
- **Inputs**: closure parameters of the standard $k-\varepsilon$ turbulence model

$$\boldsymbol{x} = \left(C_\mu, \sigma_k, \sigma_\varepsilon, C_{\varepsilon_1}, C_{\varepsilon_2}\right)$$

- **Output**: Reynolds stress tensor $\tau_{ij} = \overline{u_i' u_j'}$ and the turbulent kinetic energy k
- The incompressibility condition is translated by:

$$\boldsymbol{\tau_{11} + \tau_{22} - \frac{4}{3}k = 0}$$

Datasets generation details:

- Mesh composed of 200 000 triangular elements
- CEA/DES CFD solver TrioCFD
- Reynolds number = 18000
- N_{train} = 50 and $N_{test} = 100$

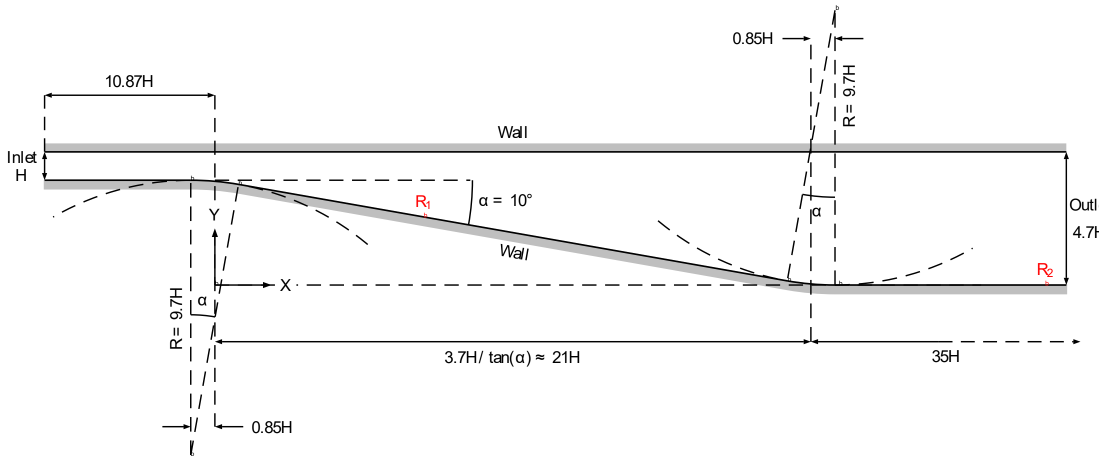

Figure: Scheme of the experiment carried out in Buice and Eaton, 2000. The wall of the channel are defined by straight lines and circular arcs of centers O_1 and O_2

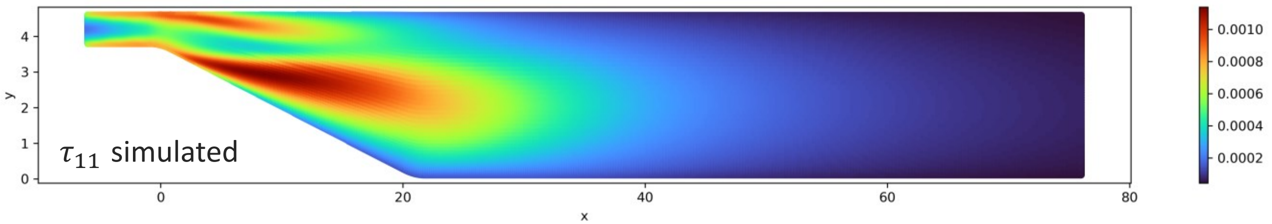

Results on the LEVM Reynolds stress tensor

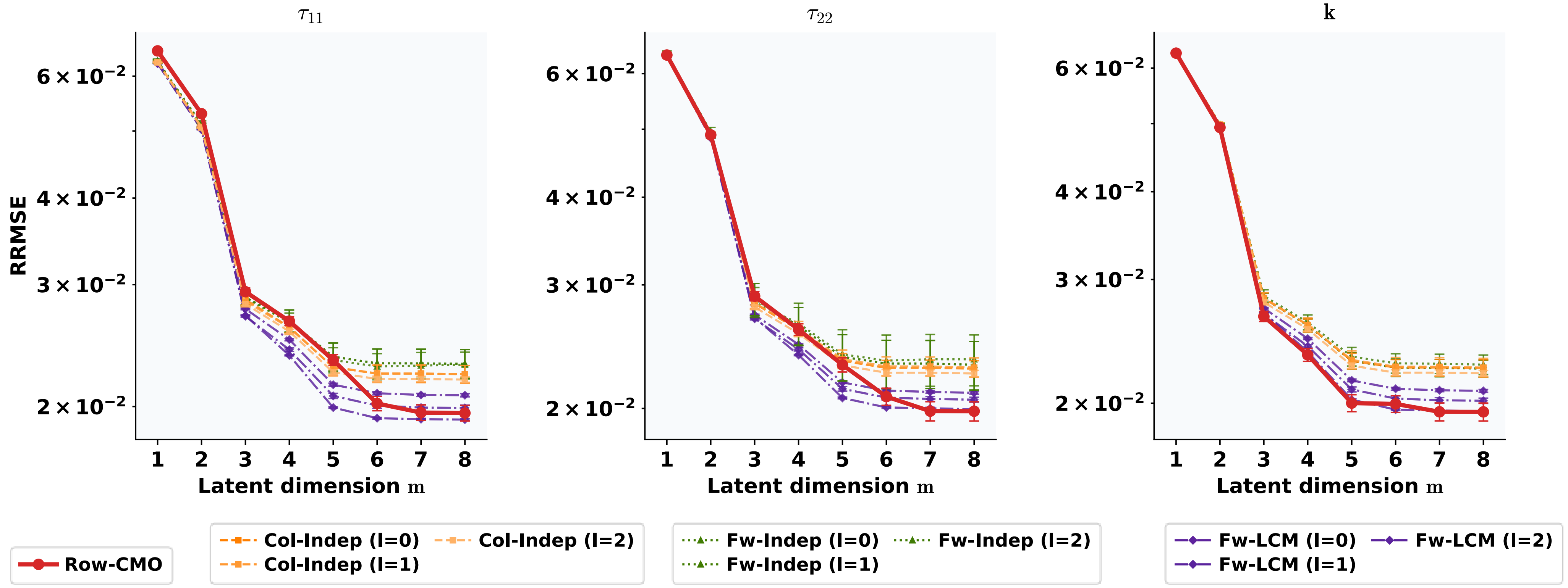

Figure: RRMSE (mean±std) on all outputs for all methods.

Appendix : Gaussian process regression

- **Single-output GP regression**[2]

$(x_i, y_i)_{\{i=1,\ldots,N\}} \in \mathcal{X} \times \mathbb{R}$, $y_i = f(x_i) + \epsilon_i$, $\epsilon_i \sim \mathcal{N}(0, \sigma^2)$

Prior: $f(x) \sim \mathcal{GP}(0, k(x, x'))$, Kernel: $k(\cdot,\cdot) : \mathcal{X} \times \mathcal{X} \to \mathbb{R}$

Posterior: $f(x_*)|y \sim \mathcal{N}(f_*, \mathrm{cov}(f_*))$

- $f_* = k_*^T (k(X,X) + \sigma^2 I)^{-1}$
- $\mathrm{cov}(f_*) = k(x_*, x_*) - k_*^T (k(X,X) + \sigma^2 I)^{-1} k_*$

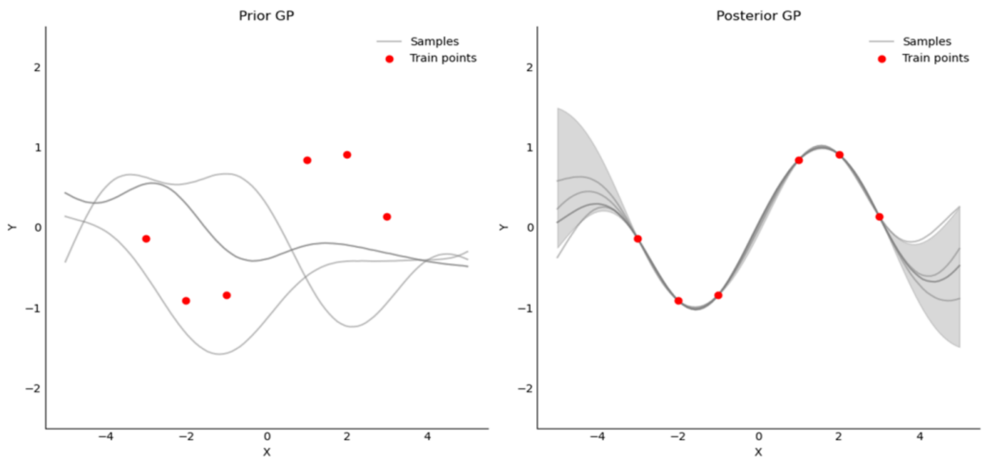

- **Multi-Output GP (MOGP)** [3]

$(x_i, \boldsymbol{y}_i)_{\{i=1,\ldots,N\}} \in \mathcal{X} \times \mathbb{R}^P$

$\boldsymbol{y}_i = \boldsymbol{f}(x_i) + \epsilon_i$, $\epsilon_i \sim \mathcal{N}(0, \Sigma)$

Prior: $\boldsymbol{f}(x) \sim \mathcal{GP}\big(0, \boldsymbol{k}(x, x')\big)$

Kernel: $\boldsymbol{k}(\cdot,\cdot) : \mathcal{X} \times \mathcal{X} \to \mathbb{R}^P \times \mathbb{R}^P$

$\rightarrow$ Matrix valued kernel

$\rightarrow$ Symmetric positive definite

Kernel models:

- Intrinsic coregionalization model

$$\boldsymbol{k}(X,X) = B \otimes k(X,X)$$

- Linear model of coregionalization

$$\boldsymbol{k}(X,X) = \sum_{q=1}^{Q} B_q \otimes k_q(X,X),$$

$B_q \in \mathbb{R}^{P \times P}, : k_q(\cdot,\cdot) : \mathcal{X} \times \mathcal{X} \to \mathbb{R}$

[2] Rasmussen, C. E. (2003)
[3] Alvarez , M. A., Rosasco, L., & Lawrence, N. D. (2012)

Appendix B

Lotka-Volterra Constraint :

- Constraint given by the Hamiltonian structure[5] of (1):
$$H(p,q) = dp - c\log(p) + bq - a\log(q) = C_0$$
- Reparametrized Hamiltonian structure:
$$\boldsymbol{dp - cs + bq - ar = C_0}$$

with $s = \log(p), r = \log(q)$

Constraint evaluation metric:

- $h(t) = \frac{1}{n_{test}} \sum_{i=1}^{n_{test}} h_i(t),$
- $h_i(t) = d\hat{p}_i(t) - c\hat{s}_i(t) + b\hat{q}_i(t) - a\hat{r}_i(t) - c_i(t)$

RRMSE metric :

$$RRMSE^2 = \frac{1}{N}\sum_{i=1}^{N} RRMSE^2(y_{sim}^i, y_{pred}^i)$$

$$RRMSE^2\left(y_{sim}^i, y_{pred}^i\right) = \frac{\left\|y_{sim}^i - y_{pred}^i\right\|_2^2}{S\left\|y_{sim}^i\right\|_\infty^2}$$

Appendix B

Uncertainty propagation

Parameters of the $k - \varepsilon$ standard turbulence model calibrated on experimental data :

- C_μ : constant
- σ_ε: The Prandtl turbulent dissipation number
- C_{ε_1}: The source term coefficient
- C_{ε_2}: The well term coefficient
- σ_k :

C_μ	σ_ε	$\sigma_{\boldsymbol{k}}$	C_{ε_1}	C_{ε_2}
0.09	1.30	1.00	1.44	1.92

Table: The usual values of the calibrated parameters

PCA for multi-field data

We provided 3 theoretical results in order to compare these three approaches:

- **Row-wise PCA vs field-wise PCA:** The excess of row-wise PCA error for a field k is guaranteed to be bounded by a small number when the **covariance matrices** of the other fields are close to that of field k

- **Col-wise PCA vs field-wise PCA:** A similar excess-error bound holds for col-wise PCA, with similarity measured through the **Gram matrices**

☛ These 2 results provide theoretical justification of using row-wise PCA and col-wise PCA over field wise when these similarities hold

- **Row-wise PCA vs col-wise PCA:** We give an exact dominance criterion which state that neither strategy is intrinsically superior

Numerical Applications

Lotka–Volterra equations — Population Dynamics

Comparison between our proposed framework row-wise PCA-Constrained MOGP and deductive alternatives based on:

- field-wise PCA
- column-wise PCA

Main findings

- Strong agreement between our proposed theoretical criterion and observed RRMSE rankings
- ➢ It can therefore be helpful in practice to evaluate how much we can loose by relying on row-wise PCA

- In data-scarce regimes, the proposed framework consistently achieves the lowest RRMSE as the latent dimension increases.